Preprint
UCRL-JC-153184

Difference approximations of the Neumann problem for the second order wave equation

Heinz-Otto Kreiss
N. Anders Petersson
Jacob Yström

This article was submitted to SIAM Journal on Numerical Analysis

May 5, 2003

DISCLAIMER

This research was supported under the auspices of the U.S. Department of Energy by the University of California, Lawrence Livermore National Laboratory under contract No. W-7405-Eng-48.

Difference approximations of the Neumann problem for the second order wave equation*

Heinz-Otto Kreiss†, N. Anders Petersson‡and Jacob Ystrom§

May 5, 2003, Revised December 2, 2003

Abstract

Stability theory and numerical experiments are presented for a finite difference method that directly discretizes the Neumann problem for the second order wave equation. Complex geometries are discretized using a Cartesian embedded boundary technique. Both second and third order accurate approximations of the boundary conditions are presented. Away from the boundary, the basic second order method can be corrected to achieve fourth order spatial accuracy. To integrate in time, we present both a second order and a fourth order accurate explicit method. The stability of the method is ensured by adding a small fourth order dissipation operator, locally modified near the boundary to allow its application at all grid points inside the computational domain. Numerical experiments demonstrate the accuracy and long-time stability of the proposed method.

1 Introduction

There are many methods to solve the wave equation numerically. Methods based on variational principles [1] have the advantage that the energy is conserved, but they are not as efficient as difference methods. On the other hand, difference methods are prone to instabilities. To avoid these one often has to add dissipative terms and the energy is not conserved. Luckily, the instabilities are often weak and caused by high frequency waves

*This work was performed under the auspices of the U.S. Department of Energy by University of California Lawrence Livermore National Laboratory under contract No. W-7405-Eng-48.

†Department of Mathematics, University of California Los Angeles, CA 90024.

‡Center for Applied Scientific Computing, Lawrence Livermore National Lab, Livermore, CA 94551, andersp@llnl.gov.

§Department of Numerical Analysis and Computing Science, Royal Institute of Technology, S-100 44 Stockholm, Sweden, yxan@nada.kth.se.

which are not accurately represented anyway. Therefore, one constructs the dissipation in such a way that it acts mainly only on these frequencies. We feel that the fixation on energy conservation often goes too far. Large phase errors can destroy the solution as well.

In this paper we continue the development of numerical methods that directly discretize the second order wave equation without first re-writing it as a system of first order equations. In particular, we want to discuss the kind of instabilities that can arise and how to control them. Since we treated the Dirichlet problem in [2], we consider here only the Neumann problem

$$\begin{aligned} u_{tt} &= \Delta u + F(\boldsymbol{x},t), \quad \boldsymbol{x}\in\Omega, \quad t>0, \\ \frac{\partial u}{\partial n}(\boldsymbol{x},t) &= f(\boldsymbol{x},t), \quad \boldsymbol{x}\in\Gamma, \quad t>0, \\ u(\boldsymbol{x},0) &= u_0(\boldsymbol{x}), \quad u_t(\boldsymbol{x},0)=u_1(\boldsymbol{x}), \quad \boldsymbol{x}\in\Omega, \end{aligned} \tag{1}$$

where Ω is a bounded one or two-dimensional domain with boundary Γ.

We will discretize (1) on a Cartesian embedded boundary grid. The embedded boundary technique for discretizing partial differential equations date back to the first order technique by Weller and Shortley [3] and the higher order generalizations of Collatz [4]. More recently, several embedded boundary methods have been presented for various types of partial differential equations. For example, Pember et al. [5] used a Cartesian grid method for solving the time-dependent equations of gas dynamics. Zhang and LeVeque [6] solved the acoustic wave equation with discontinuous coefficients written as a first order system. They derived special difference stencils that satisfy the jump conditions at the interior interfaces, where the coefficients are discontinuous. A staggered grid method was used by Ditkowski, Dridi and Hesthaven [7] for solving Maxwell's equations on a Cartesian grid. The methods described in these papers all solve first order systems (in time). For Poisson's equation with Dirichlet boundary conditions, Johansen and Colella [8] derived an embedded boundary technique based on the finite volume method combined with multi-grid.

We proceed by presenting the highlights of our proposed method. The domain Ω is covered by a Cartesian grid with step size h where the grid points are located at $\boldsymbol{x}_{i,j} = (x_i, y_j)^T = (ih, jh)^T$, and the boundary Γ is allowed to cut through the grid in an arbitrary manner, see Figure 1. Let $t_n = nk$, $k = 0, 1, 2, \ldots$ denote the time-discretization with step size k, and let $v^n_{i,j}$ be the difference approximation of $u(x_i, y_j, t_n)$. A second order accurate approximation of the Laplacian of u is given by

$$\Delta_h v^n_{i,j} =: \frac{1}{h^2}(v^n_{i+1,j} + v^n_{i-1,j} + v^n_{i,j+1} + v^n_{i,j-1} - 4v^n_{i,j}). \tag{2}$$

To be able to evaluate $\Delta_h v^n_{i,j}$ at all grid points inside Ω, we use ghost points just outside the domain. Consider the case in Figure 1 where the grid point $\boldsymbol{x}_{i,j}$ is outside of Ω, but $\boldsymbol{x}_{i,j+1}$ is inside. To aid in the approximation of the Neumann boundary condition,

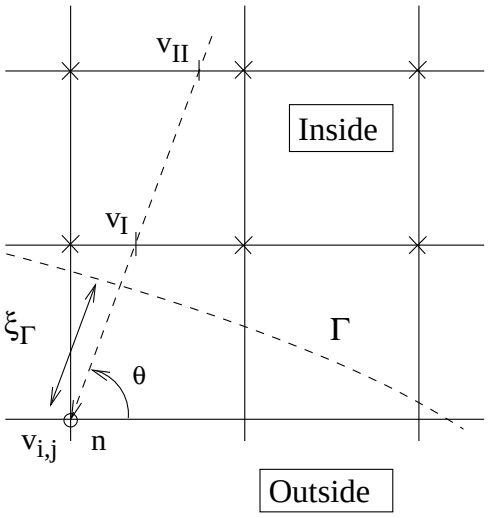

Figure 1: The points used for discretizing the Neumann boundary condition.

we construct a third order accurate interpolant between three points along the normal: $(0, v^n_{i,j})$, (ξ_I, v^n_I), (ξ_{II}, v^n_{II}). Here ξ_I and $\xi_{II} = 2\xi_I$ are the distances between $\boldsymbol{x}_{i,j}$, along the normal going through that point, and the horizontal grid lines y_{j+1} and y_{j+2}, respectively. After differentiating the interpolant, we get a second order accurate approximation of the (outward) normal derivative

$$D^{(2)}_n v^n_{i,j} =: g_0 v^n_{i,j} + g_I v^n_I + g_{II} v^n_{II} = \frac{\partial v}{\partial n}(\boldsymbol{x}^\Gamma_{i,j}, t_n) + O(h^2), \tag{3}$$

where $\boldsymbol{x}^\Gamma_{i,j}$ is the intersection point between the boundary and the normal going through $\boldsymbol{x}_{i,j}$. The coefficients g_j are given by

$$g_0 = \frac{3\xi_I - 2\xi_\Gamma}{2\xi_I^2}, \quad g_I = \frac{2\xi_\Gamma - 2\xi_I}{\xi_I^2}, \quad g_{II} = \frac{\xi_I - 2\xi_\Gamma}{2\xi_I^2}, \tag{4}$$

where ξ_Γ is the distance between $\boldsymbol{x}_{i,j}$ and the boundary. Since the coefficients $g_j = \mathcal{O}(1/h)$, we need to use third order accurate approximations for v^n_I and v^n_{II}. Here we use Lagrangian interpolation along the grid lines y_{j+1} and y_{j+2}:

$$\begin{aligned} v^n_I &= c_0 v^n_{i,j+1} + c_1 v^n_{i+1,j+1} + c_2 v^n_{i+2,j+1}, \\ v^n_{II} &= c_3 v^n_{i,j+2} + c_4 v^n_{i+1,j+2} + c_5 v^n_{i+2,j+2}. \end{aligned}$$

The resulting formula for $D^{(2)}_n v_{i,j}$ holds when the angle θ between the x-axis and the normal satisfies $\pi/4 \le \theta \le \pi/2$. When $0 \le \theta \le \pi/4$, the horizontal interpolations to obtain v_I and v_{II} are replaced by corresponding interpolations in the vertical direction. The expressions in the remaining three quadrants are simply obtained by reflections in

index space, leading to a total of 8 different cases to treat all possible directions of the boundary.

The second order boundary condition formula results in an overall second order scheme, but since the boundary condition is discretized using one-sided differences, the truncation error will be larger at the boundary than in the interior, where a centered scheme is used. We can easily modify the above technique to construct a third order accurate formula $D_n^{(3)} v_{i,j}$ to make the coefficient in front of the leading second order truncation error term smaller. In this case, three interior values v_I, v_{II}, and v_{III} are interpolated using fourth order Lagrangian interpolation along three contiguous grid lines. Hence this stencil involves 12 interior points. The third order boundary condition formula works nicely for well resolved geometries where there are enough interior points. For less resolved geometries, or for very thin regions where two parts of the boundary are close to each other, we will use the second order boundary condition formula.

All ghost point values in (2) can be eliminated using formulas of the type (3). The discrete approximation of the Laplacian of u (for functions subject to the boundary condition $\partial u/\partial n = f(\boldsymbol{x}^\Gamma, t)$) can then be written in matrix form

$$\Delta u = A\boldsymbol{v} + \boldsymbol{b}(t) + O(h^2). \tag{5}$$

Here the array $\boldsymbol{v}$ contains the solution at all grid points inside Ω and $\boldsymbol{b}(t)$ is the discrete counterpart of the boundary forcing $f(\boldsymbol{x}_\Gamma, t)$.

Because of the discretized form of the Neumann boundary condition, the matrix A will not be symmetric. As a result, the basic scheme proposed in [2],

$$\frac{\boldsymbol{v}^{n+1} - 2\boldsymbol{v}^n + \boldsymbol{v}^{n-1}}{k^2} = A\boldsymbol{v}^n + \boldsymbol{b}(t_n) + \boldsymbol{F}(t_n),$$

suffers from a weak instability (here $\boldsymbol{F}(t_n)$ is the discretized version of the internal forcing $F(\boldsymbol{x}, t_n)$). The definition of a weak instability will be given in Section 4. To understand the loss of stability, we analyze a number of model problems. We start with the one-dimensional half-plane (§ 2) and strip (§ 3) problems, proving that the difference approximation is stable in these cases, without damping. The two-dimensional case is analyzed in Sections 4-6, where we show that the tangential derivatives that occur in the truncation error of the boundary condition can lead to instabilities, both for the half-plane and strip problems. We also show that our scheme can be stabilized by a small fourth order artificial dissipation of the type $h^3\Delta^2\boldsymbol{v}_t$. However, a centered finite difference stencil such as $\Delta_h^2\boldsymbol{v}_t$ is wider than the discretized Laplacian, so it is not possible to use this damping term all the way up to the boundary (without adding extra numerical boundary conditions). Instead, we suggest using the discrete operator $h^3 A^T(A(\boldsymbol{v}^n - \boldsymbol{v}^{n-1})/k)$ which *can* be applied all the way up to the boundary. Away from the boundary, it is equivalent to $\Delta_h^2(\boldsymbol{v}^n - \boldsymbol{v}^{n-1})/k$. For the general case with inhomogeneous boundary conditions and internal forcing, the proposed scheme becomes

$$\frac{\boldsymbol{v}^{n+1} - 2\boldsymbol{v}^n + \boldsymbol{v}^{n-1}}{k^2} = A\boldsymbol{v}^n + \boldsymbol{b}(t_n) + \boldsymbol{F}(t_n) - \alpha h^3 A^T \left(A(\boldsymbol{v}^n - \boldsymbol{v}^{n-1})/k + \frac{d\boldsymbol{b}}{dt}(t_n) \right). \tag{6}$$

We note that the sparse structure of A can be used to efficiently evaluate both $A\boldsymbol{v}$ and $A^T\boldsymbol{v}$, without the need to store the matrix explicitly, see appendix A.

In Section 7.1, we will demonstrate that this discretization does not suffer from the "small cell" stiffness problem that commonly is encountered when the finite volume method is used on a Cartesian grid with an embedded boundary, cf. [9]. We will also show that the damping term inflicts an $\mathcal{O}(h^2)$ perturbation of the undamped scheme (§ 7.2), and by numerical experiments in Section 8 we will demonstrate that it suffices to take α very small (of the order $\mathcal{O}(10^{-3})$). Hence, the resulting numerical solution will be second order accurate and the scheme is well suited for long time calculations where it is important to keep damping to a minimum. In Section 7.3, we also present correction terms that optionally can be added to make the scheme fourth order accurate in time and space (away from the boundary). A number of numerical examples are presented in Section 8 to asses the accuracy and long time stability of the method with and without fourth order corrections, both for smooth boundaries and in the presence of corners. The proposed method is finally used for a resonance analysis of wave propagation in a harbor.

2 The one-dimensional half-plane problem

We start with the half-plane problem

$$\begin{aligned} u_{tt} &= u_{xx}, \quad 0 \le x < \infty,\ t \ge 0, \\ u(x,0) &= f(x), \end{aligned} \tag{7}$$

with boundary conditions

$$u_x(0,t) = 0, \quad \lim_{x\to\infty} u(x,t) = 0. \tag{8}$$

Let $x_\nu = \nu h,\ h > 0$, denote the grid points, $v(x_\nu, t)$ be a grid function, and $D_+v(x_\nu,t) = \big(v(x_{\nu+1},t) - v(x_\nu,t)\big)/h$ represent the usual forward difference operator. We want to solve (7),(8) by the simplest central difference approximation

$$\begin{aligned} v_{tt}(x_\nu,t) &= D_+D_-v(x_\nu,t), \quad \nu = 1,2,\dots, \\ v(x_\nu,0) &= f(x_\nu), \end{aligned} \tag{9}$$

with boundary conditions

$$D_+v(0,t) + \alpha h D_+^2 v(0,t) + \beta h^2 D_+^3 v(0,t) = 0, \quad \lim_{x_\nu\to\infty} v(x_\nu,t) = 0. \tag{10}$$

If we set $\alpha = \beta = 0$ or $\alpha = -\frac{1}{2},\ \beta = 0$, we obtain a first order or second order accurate approximation, respectively. In these cases we can prove stability by energy estimates, see [2]. If $\alpha = -\frac{1}{2}$ and $\beta = \frac{1}{3}$, we obtain the third order accurate approximation

$$D_+v(0,t) - \frac{1}{2}hD_+^2v(0,t) + \frac{1}{3}h^2D_+^3v(0,t) = 0. \tag{11}$$

In this case, we do not know how to prove stability by energy estimates. Instead, we will use mode analysis.

For simplicity, we keep time continuous. In actual calculations we use the method of lines. In [10] we have shown that the stability of the semi-discrete approximation implies the stability of the totally discretized method for most standard methods of lines.

By stability we mean here that there are no exponentially growing solutions. Therefore, a test for stability is that (9),(10) has no solutions of type

$$v(x_\nu, t) = e^{st}\varphi(x_\nu), \quad |\varphi(x_\nu)| \leq \text{ const.} \tag{12}$$

for $\text{Re } s > 0$, satisfying the boundary condition (10). Introducing (12) into (9) gives us

$$h^2 s^2 \varphi(x_\nu) = h^2 D_+ D_- \varphi(x_\nu) = \varphi(x_\nu + h) - 2\varphi(x_\nu) + \varphi(x_\nu - h). \tag{13}$$

Since (13) is a difference equation with constant coefficients, its general solution is of the form

$$\varphi(x_\nu) = \sigma_1 \kappa_1^\nu + \sigma_2 \kappa_2^\nu, \tag{14}$$

where κ_1, κ_2 are solutions of the characteristic equation

$$(\kappa - 1)^2 - h^2 s^2 \kappa = 0. \tag{15}$$

We have $\kappa_2 = \kappa_1^{-1}$ and we simplify the notation by removing the index of the roots and set $\kappa_1 = \kappa$, $\kappa_2 = \kappa^{-1}$.

Lemma 1 *For $|hs| \ll 1$, the roots of (15) are of the form*

$$\begin{aligned} \kappa &= 1 - hs + \tfrac{h^2 s^2}{2} + \mathcal{O}(h^3 s^3) = e^{-hs(1+\mathcal{O}(h^2 s^2))}, \\ \kappa^{-1} &= 1 + hs + \tfrac{h^2 s^2}{2} + \mathcal{O}(h^3 s^3) = e^{hs(1+\mathcal{O}(h^2 s^2))}. \end{aligned} \tag{16}$$

Also, for $\text{Re } s > 0$, (15) has no root with $|\kappa| = 1$ and exactly one root κ with $|\kappa| < 1$.

Proof. (16) follows by asymptotic expansion of the roots. (It is not surprising: The corresponding solutions of (7) are e^{-sx}, e^{sx} and (9) is second order accurate.)

Assume that (15) has a solution

$$|\kappa| = 1, \quad \text{i.e.,} \quad \kappa = e^{i\tau}, \ \tau \text{ real},$$

for some s with $\text{Re } s > 0$. Then (15) becomes

$$-4\sin^2(\tau/2) = h^2 s^2.$$

Therefore, $\text{Re } s = 0$, which is a contradiction.

For $hs \to \infty,\ s > 0$ real, the solutions of (15) satisfy

$$\lim_{hs\to\infty} \kappa = 0, \quad \lim_{hs\to\infty} \kappa^{-1} = \infty.$$

Since the roots are smooth functions of s and $|\kappa| \neq 1$ for Re $s > 0$, we always have $|\kappa| < 1,\ |\kappa^{-1}| > 1$. This proves the lemma.

The lemma shows that the solution can only stay bounded in space if $\sigma_2 = 0$, so

$$\varphi(x_\nu) = \sigma_1 \kappa^\nu, \quad |\kappa| < 1. \tag{17}$$

Introducing (17) into the boundary condition (10) gives us

$$(\kappa - 1)\left(1 + \alpha(\kappa - 1) + \beta(\kappa - 1)^2\right) = 0. \tag{18}$$

The cubic equation (18) has three roots $\kappa = \kappa_j,\ j = 1, 2, 3$, which lead to possible solutions of (12). We obtain the corresponding s from the characteristic equation (15), i.e.,

$$hs = \pm\sqrt{\frac{(\kappa - 1)^2}{\kappa}} = \pm(\kappa^{1/2} - \kappa^{-1/2}). \tag{19}$$

The first root, $\kappa_1 = 1$, does not generate a growing solution. In fact, any root with $|\kappa| = 1$, has this property, since inserting $\kappa = e^{i\xi}$ into (19) yields

$$hs = \pm 2i \sin\frac{\xi}{2}, \text{ i.e., } \text{Re } s = 0. \tag{20}$$

Roots with $|\kappa| > 1$, are not permissible because $\varphi(x_\nu) = \sigma\kappa^\nu$ becomes unbounded as $\nu \to \infty$ and violates the boundary condition (10). However, solutions of the type, $\kappa = e^{i\xi - \eta},\ \xi, \eta$ real, $\eta > 0$ correspond to

$$h \text{ Re } s = \pm(e^{-\eta/2} - e^{\eta/2}) \cos\frac{\xi}{2},$$

which grows rapidly in time if $\xi \neq \pi + 2n\pi,\ n = 0, 1, 2, \ldots$. These solutions decay rapidly away from the boundary, and we therefore denote these solutions *boundary layer instabilities*.

Often one tries to stabilize numerical methods by adding a dissipative term to the difference equation. Instead of (9) we then consider

$$v_{tt} = D_+ D_- v + \sigma h D_+ D_- v_t.$$

For boundary layer instabilities, this does not work. If the boundary layer is oscillatory, then one can stabilize the method but the amount of necessary dissipation is, in general, too large for accuracy reasons. Therefore, the only useful boundary condition approximations are those where $|\kappa_2| > 1,\ |\kappa_3| > 1$. While this condition is violated for general coefficients α, β, it is easy to see that the third order approximation (11) satisfies the requirement. That approximation has $\alpha = -\frac{1}{2},\ \beta = \frac{1}{3}$, and (18) has the solutions

$$\kappa_1 = 1, \quad \kappa_{2,3} = \frac{7}{4} \pm i\sqrt{3 - \frac{9}{16}}, \quad |\kappa_{2,3}| = \frac{\sqrt{88}}{4} > \frac{9}{4}. \tag{21}$$

3 The one-dimensional strip problem

We consider now the wave equation (7) for $0 \le x \le 1,\ t \ge 0$. As boundary conditions we use

$$u_x(0,t) = 0, \quad u(1,t) = 0. \tag{22}$$

We approximate the continuous problem by

$$\begin{aligned} v_{tt}(x_\nu,t) &= D_+D_-v(x_\nu,t), \quad \nu = 1,2,\ldots,N-1,\ Nh = 1, \\ v(x_\nu,0) &= f(x_\nu), \end{aligned} \tag{23}$$

with boundary conditions

$$\begin{aligned} L_hv =: D_+v(0,t) - \tfrac{1}{2}hD_+^2v(0,t) + \tfrac{1}{3}h^2D_+^3v(0,t) = 0, \\ v(1,t) \ = \ 0. \end{aligned} \tag{24}$$

For the analytic problem (7),(22) there is an energy estimate. Also, we can represent the solution by an eigenfunction expansion

$$u(x,t) = \sum_{j=0}^{\infty} e^{\lambda_j t}\psi_j(x).$$

The eigenvalues λ_j are purely imaginary and are solutions of the eigenvalue problem

$$\lambda^2\psi = \psi_{xx}, \quad \psi_x(0) = \psi(1) = 0. \tag{25}$$

Again we want to investigate whether (23),(24) has exponentially growing solutions. We make the ansatz (12) and obtain

$$\begin{aligned} h^2s^2\varphi(x_\nu) &= h^2D_+D_-\varphi(x_\nu), \\ L_h\varphi = 0, &\quad \varphi(1) = 0, \end{aligned} \tag{26}$$

and start our discussion with the case that $|sh| << 1$. The discretized eigenvalue problem (26) is an approximation of the continuous problem (25) and since the difference stencil is compact, solutions of (26) with $|sh| << 1$ are close to solutions of the continuous problem, see Kreiss [11]. The question is whether the eigenvalues also are purely imaginary.

The general solution of (26) is

$$\varphi(x_\nu) = \sigma_1\kappa_1^\nu + \sigma_2\kappa_2^\nu, \tag{27}$$

where $\kappa_j,\ j = 1,2$, are the solutions of the characteristic equation (15)

$$\kappa^2 - (2 + h^2s^2)\kappa + 1 = 0.$$

Therefore $\kappa_1\kappa_2 = 1$, i.e., $\kappa_2 = \kappa_1^{-1}$. By (16) we can write

$$\kappa_1 = e^{h\tilde{s}}, \quad \kappa_2 = e^{-h\tilde{s}}, \quad \tilde{s} =: s(1 + \mathcal{O}(h^2 s^2)),$$

and

$$\varphi(x) = \sigma_1 e^{\tilde{s}x} + \sigma_2 e^{-\tilde{s}x}, \quad x = x_\nu,\ \nu = 0, 1, 2, \ldots, N,\ Nh = 1.$$

For smooth functions $w(x)$,

$$L_h w = w_x(0) + \gamma_4 h^3 w_{xxxx}(0) + \gamma_5 h^4 w_{xxxxx}(0) + \mathcal{O}(h^5).$$

Therefore, introducing (27) into the boundary conditions gives us

$$\sigma_1(1 + \tilde{\gamma}_4 h^3 \tilde{s}^3 + \tilde{\gamma}_5 h^4 \tilde{s}^4) - \sigma_2(1 - \tilde{\gamma}_4 h^3 \tilde{s}^3 + \tilde{\gamma}_5 h^4 \tilde{s}^4) = 0, \tag{28}$$

$$\sigma_1 e^{\tilde{s}} + \sigma_2 e^{-\tilde{s}} = 0. \tag{29}$$

Here

$$\tilde{\gamma}_4 = \gamma_4 + \gamma_{41}\tilde{s}^2 h^2 + \ldots, \quad \tilde{\gamma}_5 = \gamma_5 + \gamma_{51}\tilde{s}^2 h^2 + \ldots,$$

account for the higher order terms.

There is a nontrivial solution of (28),(29) if and only if

$$\frac{\sigma_2}{\sigma_1} = -e^{2\tilde{s}} = \frac{1 + \tilde{\gamma}_5 h^4 \tilde{s}^4 + \tilde{\gamma}_4 h^3 \tilde{s}^3}{1 + \tilde{\gamma}_5 h^4 \tilde{s}^4 - \tilde{\gamma}_4 h^3 \tilde{s}^3}.$$

If $|sh| \ll 1$, then the eigenvalues of (26) converge to the eigenvalues $\lambda_n = i(\frac{\pi}{2} + n\pi)$ of (25) where $|h\lambda_n| \ll 1$. Thus we make the ansatz

$$h\tilde{s} = h\lambda_n + ih\tau = ih\mu_n + ih\tau, \quad \mu_n = \frac{\pi}{2} + n\pi,$$

and obtain

$$e^{2i\tau} = \frac{1 + \tilde{\gamma}_5\big((\mu_n + \tau)h\big)^4 - i\tilde{\gamma}_4\big((\mu_n + \tau)h\big)^3}{1 + \tilde{\gamma}_5\big((\mu_n + \tau)h\big)^4 + i\tilde{\gamma}_4\big((\mu_n + \tau)h\big)^3} =: S. \tag{30}$$

Since $\tilde{\gamma}_4, \tilde{\gamma}_5$ are real and bounded and μ_n is real, an asymptotic expansion of $|S|$ in h yields

$$|S| = 1 + \mathcal{O}(|\tau|^3 h^3) = e^{2i\tau}.$$

Hence, τ must be real-valued, that is, $\tilde{s}$ must be purely imaginary. By the above expansion, it follows that there is a unique solution close to λ_n with

$$i\tau = i\tilde{\gamma}_4(\mu_n h)^3 + \mathcal{O}\big((\mu_n h)^4\big),\ \tau \text{ real}.$$

Thus the eigenvalues of the discrete problem are purely imaginary, provided $|sh| \ll 1$.

Now we consider the case that $|sh| \geq \tilde{\delta} > 0$. The characteristic equation (15) implies

$$|\kappa - 1|^2 = |sh|^2|\kappa| \geq \tilde{\delta}^2|\kappa|.$$

Hence, when $|\kappa| \geq 1/2$,

$$|\kappa - 1| \geq \tilde{\delta}/\sqrt{2} = \delta > 0.$$

Furthermore, when $|\kappa| \leq 1/2$, the triangle inequality gives $|1 - \kappa| \geq 1 - |\kappa| \geq 1/2$. Thus κ cannot be arbitrary close to 1 when $|sh| \geq \tilde{\delta} > 0$.

In the following, we use the representation

$$\varphi(x_\nu) = \sigma_1 \kappa^{+\nu} + \sigma_2 \kappa^{-\nu}, \quad |\kappa| \geq 1.$$

The discrete eigenvalue problem (26) has a nontrivial solution if and only if

$$\sigma_1 P_h(\kappa - 1) + \sigma_2 P_h(\kappa^{-1} - 1) = 0, \quad \sigma_1 \kappa^N + \sigma_2 \kappa^{-N} = 0,$$

i.e.,

$$\kappa^N P_h(\kappa^{-1} - 1) - \kappa^{-N} P_h(\kappa - 1) = 0. \tag{31}$$

has a nontrivial solution. Here

$$P_h(y) = y - \frac{1}{2}y^2 + \frac{1}{3}y^3 \equiv y(y - y_2)(y - y_3), \quad y_{2,3} = \frac{3}{4} \pm i\sqrt{3 - \frac{9}{16}}. \tag{32}$$

Lemma 2 *There is a constant $C > 0$ such that (31) has no solution for*

$$|\kappa| \geq e^{Ch}$$

Proof. Assume that $|\kappa| = e^{Ch}$. By (32), the zeros of $P_h(y)$ are $y = 0$ and $y = y_{2,3}$ with $\mathrm{Re}\, y_{2,3} = 3/4$. For $|\kappa - 1| \geq \delta$ and $|\kappa| \geq 1$, κ^{-1} is inside the unit circle, but bounded away from 1. Therefore, $\kappa^{-1} - 1$ is inside a unit circle centered at -1, but bounded away from zero. There are no zeros of P_h in this region and we have

$$\min_{|\kappa| \geq 1,\ |\kappa - 1| \geq \delta} |P_h\left(\kappa^{-1} - 1\right)| \geq d > 0.$$

Since $|\kappa|^N = e^C$, and $\kappa^{-3} P_h(\kappa - 1) \leq$ const. for $|\kappa| \geq 1$,

$$\begin{aligned} |\kappa^{-N} P_h(\kappa - 1)| &= |\kappa^{-N+3}|\, |\kappa^{-3} P_h(\kappa - 1)| \leq \text{ const. } e^{-C}, \\ |\kappa^N P_h\left(\kappa^{-1} - 1\right)| &\geq d e^C. \end{aligned}$$

Hence, equation (31) has no solution if C is sufficiently large and the lemma follows.

We can now prove

Theorem 1 *For sufficiently small h, all eigenvalues s of (26) are purely imaginary and the discrete problem (23),(24) is stable.*

Proof. We have already shown that all eigenvalues with $|sh| \ll 1$ are purely imaginary. For $|sh| \geq \tilde{\delta}$, the eigenvalue problem (26) has a solution if and only if (31) has a solution with $|\kappa| \geq 1$ and $|\kappa - 1| \geq \delta$. We can write (31) in the form

$$Q(\kappa) =: \frac{P_h(\kappa^{-1} - 1)}{P_h(\kappa - 1)} = \kappa^{-2N}. \tag{33}$$

By noting that $\overline{P_h(y)} = P_h(\overline{y})$ and that $\overline{e^{i\xi} - 1} = e^{-i\xi} - 1$, it is easy to see that

$$|Q(e^{i\xi})| = 1, \quad \left|(e^{i\xi})^{-2N}\right| = 1.$$

Now consider $\kappa = e^{i\xi + \eta h},\ 0 \leq \eta \leq C$. Then,

$$|Q(e^{i\xi+\eta h})| = 1 + \mathcal{O}(\eta h), \text{ but } \left|(e^{i\xi+\eta h})^{-2N}\right| = e^{-2\eta}. \tag{34}$$

For sufficiently small h, (33) can only have solutions for $\eta = 0$ since only the left hand side of (34) scales with h. Lemma 2 tells us that (31) has no solution for $|\kappa| \geq e^{Ch}$, and we conclude that all solutions of (31) must have $|\kappa| = 1$. By solving the characteristic equation (15) for s and setting $\kappa = e^{i\xi}$, we get (20) which shows that all eigenvalues are purely imaginary.

Since we can represent the solution of the discrete problem (23),(24) in an eigenfunction expansion where all eigenvalues are purely imaginary, there can be no exponentially growing solutions and we conclude that the discrete problem is stable.

4 A continuous two-dimensional model problem

We now start our discussion of two-dimensional problems. The results from the one-dimensional model seems to indicate that we need only to avoid boundary instabilities. However, there are also highly oscillatory instabilities which can be controlled by small amounts of dissipation. As will be demonstrated in Section 5, our embedded boundary approximation of the Neumann condition in general two-dimensional domains introduces truncation errors in both the tangential and normal directions. To illustrate the type of instabilities that the tangential terms can give, we study the solutions of the wave equation with perturbed Neumann conditions. We start with the half-plane problem

$$\begin{aligned} u_{tt} &= u_{xx} + u_{yy}, \quad 0 \leq x < \infty, \ -\infty < y < \infty, \ t \geq 0, \\ u_x(0, y, t) &= \epsilon u_y(0, y, t), \end{aligned} \tag{35}$$

where ϵ is a real parameter. It turns out the size of ϵ is of minor importance, and we will for simplicity consider the case $\epsilon = 1$. Corresponding to Section 2, the problem is unstable if we can find exponentially growing solutions of type

$$u = e^{st + i\omega y}\varphi(x), \quad \text{Re } s > 0, \quad |\varphi(x)| \leq \text{ const.}, \quad \omega \text{ real.} \tag{36}$$

Introducing (36) into (35) gives us the eigenvalue problem for s

$$\begin{aligned} \varphi_{xx} &= (s^2+\omega^2)\varphi, \\ \varphi_x(0) &= i\omega\varphi(0), \quad |\varphi(x)| \leq \text{ const.} \end{aligned} \tag{37}$$

Since (37) is a differential equation with constant coefficients, its general solution is

$$\varphi(x) = \sigma_1 e^{\lambda x} + \sigma_2 e^{-\lambda x}, \quad \lambda = \sqrt{s^2+\omega^2}, \quad \operatorname{Re}\lambda \geq 0. \tag{38}$$

Clearly, $\operatorname{Re}\lambda > 0$ for $\operatorname{Re} s > 0$. Therefore, $|\varphi(x)| \leq$ const. if and only if $\sigma_1 = 0$, i.e.,

$$\varphi(x) = \sigma_2 e^{-\lambda x}, \quad \operatorname{Re}\lambda > 0. \tag{39}$$

Introducing (39) into the boundary condition gives us

$$-\lambda = i\omega.$$

Since $\operatorname{Re}\lambda > 0$, there are no solutions of type (36). However, let $s = i\sqrt{2}\,\omega + \eta,\ \eta > 0$. Solving (38) for λ gives

$$\lim_{\eta\to 0} \lambda = i|\omega|.$$

Thus, for $\omega < 0$, there is a solution of type (36) but with $\operatorname{Re} s = 0$,

$$u = e^{i\sqrt{2}\,\omega t - i|\omega|(x+y)}. \tag{40}$$

There is no exponential growth in time and, for large ω, the solutions are highly oscillatory in space. Furthermore, there is no decay in the x-direction. Hence, $s = i\sqrt{2}\omega$ is a generalized eigenvalue (see [12] for a definition) which forecasts instabilities for the corresponding problem on a bounded domain.

To demonstrate these instabilities, we next consider the strip problem,

$$\begin{aligned} u_{tt} &= u_{xx} + u_{yy}, \quad 0 \leq x \leq 1, \ -\infty < y < \infty, \ t \geq 0, \\ u_x(0,y,t) &= u_y(0,y,t), \quad u_x(1,t) = 0. \end{aligned} \tag{41}$$

Again, we construct solutions of the type (36). Instead of (37), we obtain now the eigenvalue problem

$$\begin{aligned} \varphi_{xx} &= (s^2+\omega^2)\varphi, \\ \varphi_x(0) &= i\omega\varphi(0), \quad \varphi_x(1) = 0. \end{aligned} \tag{42}$$

Introducing the general solution (38) into the boundary conditions shows that (42) has a solution if

$$\frac{\lambda - i\omega}{\lambda + i\omega} = e^{2\lambda}. \tag{43}$$

Theorem 2 *The strip problem (41) is unstable. For large $|\omega|$ there are solutions of the type (36) with*

$$\text{Re } s \approx \frac{1}{\sqrt{8}} \log(2|\omega|), \quad \text{i.e.,} \quad e^{(Re\, s)t} = (2|\omega|)^{t/\sqrt{8}}. \tag{44}$$

Proof. Let

$$\lambda = \lambda_r + i\lambda_i,$$

and assume that

$$\lambda_i = -\omega, \quad |\omega| \gg 1.$$

By (43),

$$\frac{\lambda_r - 2i\omega}{\lambda_r} = e^{2\lambda_r} e^{-2i\omega}. \tag{45}$$

Take $|\omega|$ large and $\arg \omega$ such that the argument of the left and right hand side of (45) match. The modulus matches if

$$\frac{\lambda_r^2 + 4\omega^2}{\lambda_r^2} = e^{4\lambda_r},$$

i.e., to the highest order in ω,

$$\lambda_r \approx \frac{1}{2} \log(2|\omega|).$$

Thus,

$$s = \pm\sqrt{-\omega^2 + \lambda^2} \approx \pm\sqrt{-2\omega^2 - i\omega \log(2|\omega|)},$$

and (44) follows.

The above example shows that the stability of the left and right half-plane problems is not enough to insure stability for the strip problem. The reason is that the generalized eigenfunctions (40) do not decay in space but are reflected back and forth between the boundaries at $x = 0, 1$, respectively. Every time they hit the left boundary they are amplified. These are highly oscillatory instabilities and we will see that they can easily be controlled by small amounts of dissipation. This example also illustrates that non-dissipative difference methods of our type are prone to weak instabilities, i.e., instabilities that only grow algebraically in time (see (44)). Note that a weak instability also occurs if the tangential derivative in (35) is replaced by a higher order, odd, tangential derivative.

To demonstrate a strong instability, we study the half-plane problem where the boundary condition in (35) is replaced by

$$u_x = \beta u_{yy}, \quad x = 0, \tag{46}$$

where β is a constant. As before, we look for solutions of the type (36) and using the same arguments as above, we know the solution must have the form (39). Inserting this ansatz into the boundary condition (46) gives

$$-\lambda = -\beta\omega^2. \tag{47}$$

Since $\mathrm{Re}\,\lambda > 0$, there are no solutions with $\mathrm{Re}\ s > 0$ when $\beta < 0$. Next we investigate if there are any generalized eigenvalues. Setting $s = i\tau$ yields $\lambda = \sqrt{-\tau^2 + \omega^2}$, so $-\lambda$ is either real and negative, or purely imaginary. When $\beta < 0$, the right hand side of (47) is always real and positive, and we conclude that there are not any generalized eigenvalues either. Hence, the case $\beta < 0$ is stable.

When $\beta > 0$ and ω is large, (47) is solved by

$$s \approx \beta\omega^2,$$

and inserting (47) into (39) gives

$$u = e^{\beta\omega^2 t - \beta\omega^2 x + i\omega y}, \quad \omega \text{ large}, \ \beta > 0.$$

Hence, these solutions have a thin boundary layer in space and grow exponentially in time. This is a strong instability. As we shall see in Section 5, this type of instability can only be controlled by dissipation when the coefficient β is small. Perturbing the Neumann condition by a higher order, even, tangential derivative results in the same behavior, i.e., the stability depends on the sign of the coefficient.

5 The discrete half-plane problem in two dimensions

We consider next the two-dimensional half-plane problem for

$$u_{tt} = u_{xx} + u_{yy}, \quad 0 \le x < \infty, \ -\infty < y < \infty, \ t \ge 0, \tag{48}$$

with the boundary condition

$$u_x(0, y, t) = 0, \quad |u(x, y, t)| \le \text{ const.}\,, \tag{49}$$

and approximate it by

$$v_{tt} = (D_{+x}D_{-x} + D_{+y}D_{-y})v, \tag{50}$$

with the third order accurate boundary condition (11)

$$L_h v(0, y, t) = 0, \quad |v(x, y, t)| \le \text{const.} \tag{51}$$

Here v is a discrete function varying on a grid

$$\{x_\nu = \nu h, \ y_\mu = \mu h\}, \quad \nu = 0, 1, 2, \ldots, \quad \mu = 0, \pm 1, \pm 2, \ldots..$$

We Fourier transform the difference equation with respect to y and obtain

$$\begin{aligned} \hat{v}_{tt} &= \left(D_{+x}D_{-x} - \tfrac{4}{h^2}\sin^2(\omega h/2)\right)\hat{v}, \\ L_h\hat{v}(0, \omega, t) &= 0, \quad |\hat{v}(x, \omega, t)| \le \text{ const.} \end{aligned} \tag{52}$$

Thus, we obtain a 1D problem for every fixed ω and can apply mode analysis as before. Then

$$\hat{v}(x_\nu, t) = e^{st}\varphi(x_\nu), \quad \text{Re } s > 0,$$

is a solution of (52) if there are solutions $\varphi(x_\nu)$ of the eigenvalue problem

$$\left(s^2 + \frac{4}{h^2}\sin^2(\omega h/2)\right)\varphi = D_{+x}D_{-x}\varphi, \tag{53}$$

$$L_h\varphi = 0, \quad |\varphi(x)| \leq \text{ const.}, \tag{54}$$

with Re $s > 0$. The eigenvalue problem (53),(54) is of the same type as for the one-dimensional half-plane problem in section 2. In particular, the general solution has the form (14) where κ now is a solution of the two-dimensional characteristic equation

$$(\kappa - 1)^2 - \left(s^2h^2 + 4\sin^2(\omega h/2)\right)\kappa = 0. \tag{55}$$

It is straight forward to show that this characteristic equation has the same essential properties as in the one-dimensional case. To be precise, we have

Lemma 3 *For $|hs| \ll 1$ and $|h\omega| \ll 1$, the roots of (55) are of the form*

$$\kappa = 1 - h\lambda + \frac{h^2\lambda^2}{2} + \mathcal{O}(h^3\lambda^3) = e^{-h\lambda(1+\mathcal{O}(h^2\lambda^2))},$$
$$\kappa^{-1} = 1 + h\lambda + \frac{h^2\lambda^2}{2} + \mathcal{O}(h^3\lambda^3) = e^{h\lambda(1+\mathcal{O}(h^2\lambda^2))},$$

where $\lambda = \sqrt{s^2+\omega^2}$, $\text{Re}\,\lambda > 0$ for Re $s > 0$. *Also, for each fixed ω and for* Re $s > 0$, *(55) has no root with $|\kappa| = 1$ and exactly one root κ with $|\kappa| < 1$.*

Proof. Follows by straight forward generalization of Lemma 1.

Since the boundary conditions are the same as in the one-dimensional case, we can use the same arguments as in Section 2 to show that there are no solutions of (53),(54) for Re $s > 0$, which implies that there are no exponentially growing solutions of (52). Note that for the Neumann boundary condition approximation (51), the boundary normal is aligned with the x-direction.

Our goal is to construct stable difference approximations for general domains. In this case the boundary condition for the differential equation is

$$\partial u/\partial n = 0, \quad \partial/\partial n: \text{ derivative normal to the boundary}, \tag{56}$$

and in general the normal is not aligned with the mesh. In the following, we will study the continuous boundary conditions perturbed by the leading truncation error terms. In the literature this technique is often used for the Cauchy or spatially periodic problems and the truncation terms appear only in the differential equation. The obtained equation is often

called the "modified equation", see for example [13] or [14]. Here we use the technique to analyze the influence of truncation errors in the boundary conditions. The modified equation is a more accurate description of the discretized problem than the continuous problem. Or rephrased, the numerical solution approximates the modified equation to a higher order of accuracy than the continuous problem. However, the modified equation can only model low and intermediate frequencies in the discrete solution, and we rely on the dissipation to control the highest frequencies.

In Section 4 we have discussed half-plane and strip problems. The reason is this: For analytic initial boundary value problems where there are no direct energy estimates, the study of wellposedness can be reduced to the study of half-plane and strip problems. This is done in the following way. In the neighborhood of every boundary point P with tangent T_g we use a locally smooth map to transform the curved boundary locally onto T_g. Then we study the half-plane problem with T_g as the boundary. After freezing the variable coefficients we can solve the problem by Fourier-Laplace transform. If for all these half-plane problems there are no eigenvalues or generalized eigenvalues s with $\operatorname{Re} s \geq 0$, then the original problem is well posed, see Kreiss and Lorenz [15].

We shall now apply this technique to analyze the stability of the discrete problem. Let the angle θ between the outward normal and the x-axis be defined as in Figure 1. We consider the differential equation on the half-plane $\boldsymbol{n} \cdot \boldsymbol{x} \leq 0$, i.e.,

$$x \cos\theta + y \sin\theta \geq 0. \tag{57}$$

To be able to calculate the truncation error of the discrete boundary condition we assume that the solution u of the differential equation is smooth and decays rapidly to zero for $x^2 + y^2 \to \infty$, in the half-plane (57). Also, we extend it smoothly beyond the boundary such that the extended u decays rapidly to zero for $x^2 + y^2 \to \infty$ in the whole plane.

The truncation error in the third order Neumann boundary condition satisfies ($\pi/4 \leq \theta \leq \pi/2$)

$$D_n^{(3)} u(x_i, y_j) = \frac{\partial u}{\partial n}(\boldsymbol{x}_{i,j}^{\Gamma}) + C_1 h^4 \frac{\partial^5 u}{\partial n^5}(\boldsymbol{x}_{i,j}^{\Gamma}) + C_2 h^3 \frac{\partial^4 u}{\partial n^4}(\boldsymbol{x}_{i,j}^{\Gamma}) + h^4 R_1 + h^3 R_2 + O(h^5).$$

Here,

$$R_1 = \sum_{\nu=1}^{3} C_{1\nu} \frac{\partial^5 u(\tilde{x}_\nu, y_{j+\nu})}{\partial x^5}, \quad R_2 = \sum_{\nu=1}^{3} C_{2\nu} \frac{\partial^4 u(\tilde{x}_\nu, y_{j+\nu})}{\partial x^4}.$$

The terms in R_1, R_2 originate from interpolation errors in v_I, v_{II}, and v_{III}, respectively.

Derivatives with respect to x and y can be related to normal ($\partial/\partial n$) and tangential ($\partial/\partial\sigma$) derivatives. We have

$$\frac{\partial}{\partial x} = -\sin\theta \frac{\partial}{\partial \sigma} - \cos\theta \frac{\partial}{\partial n}, \quad \frac{\partial}{\partial y} = \cos\theta \frac{\partial}{\partial \sigma} - \sin\theta \frac{\partial}{\partial n}.$$

We can also use Taylor expansions to express derivatives at $(\tilde{x}_\nu, y_{j+\nu})$ in terms of derivatives at the boundary point x_{ij}^Γ. After some calculations we obtain

$$D_n^{(3)} u(x_i, y_j) = (1+R)\frac{\partial u}{\partial n} - \left(h^4 \beta_1 \frac{\partial^5 u}{\partial \sigma^5} + h^3 \beta_2 \frac{\partial^4 u}{\partial \sigma^4} \right) + \mathcal{O}\left(h^5 \frac{\partial^6 u}{\partial n^{6-j} \partial \sigma^j} \right).$$

Here R is an operator of the form

$$R = \sum_{p+q \geq 3} \beta_{pq} h^{p+q} \frac{\partial^{p+q}}{\partial n^p \partial \sigma^q}.$$

We can write the half-plane problem for the differential equation in the form

$$\begin{aligned} &\frac{\partial^2 u}{\partial t^2} = \frac{\partial^2 u}{\partial n^2} + \frac{\partial^2 u}{\partial \sigma^2}, \quad n \geq 0, \ -\infty < \sigma < \infty, \\ &\frac{\partial u}{\partial n} = 0, \quad \text{for } n = 0. \end{aligned}$$

After Fourier transforming with respect to σ and Laplace transforming with respect to t we obtain

$$\frac{\partial^2 \hat{u}}{\partial n^2} = (s^2 + \omega^2)\hat{u}.$$

Thus,

$$\hat{u} = e^{-\sqrt{s^2+\omega^2}\, n} u_0(s, \omega), \quad \frac{\partial \hat{u}}{\partial n} = -\sqrt{s^2+\omega^2}\hat{u}$$

and the Fourier-Laplace transform of $\partial/\partial n$ is $-\sqrt{s^2+\omega^2}$. After freezing the coefficients, we Fourier-Laplace transform the truncation error and obtain

$$\hat{D}_n^{(3)} = -(1+\hat{R})\sqrt{s^2+\omega^2} - (i\beta_1 h^4 \omega^5 + \beta_2 h^3 \omega^4) + \mathcal{O}\left((|\omega| + |s|)^6 h^5 \right).$$

Here,

$$\hat{R} = \sum_{p+q \geq 3} \beta_{pq} \left(-\sqrt{(hs)^2 + (h\omega)^2} \right)^p (ih\omega)^q = \mathcal{O}\big((|hs| + |h\omega|)^3 \big).$$

For $|hs| + |h\omega|$ sufficiently small, $\|\hat{R}\| \leq 1/2$, and we can write

$$\begin{aligned} \hat{D}_n^{(3)} &= (1+\hat{R}) \left(-\sqrt{s^2+\omega^2} - \frac{i\beta_1 h^4 \omega^5 + \beta_2 h^3 \omega^4}{1+\hat{R}} \right) + \mathcal{O}\left((|\omega| + |s|)^6 h^5 \right) \\ &= (1+\hat{R}) \left(-\sqrt{s^2+\omega^2} - (i\beta_1 h^4 \omega^5 + \beta_2 h^3 \omega^4) \right) + \mathcal{O}\left((|\omega| + |s|)^6 h^5 \right). \end{aligned}$$

By neglecting the $\mathcal{O}(h^5)$ term and transforming back to physical space, the boundary condition $D_n^{(3)} u = 0$ corresponds to

$$(1+R)\left(\frac{\partial u}{\partial n} - \beta_1 h^4 \frac{\partial^5 u}{\partial \sigma^5} - \beta_2 h^3 \frac{\partial^4 u}{\partial \sigma^4} \right) = 0.$$

By assumption, $\|R\|$ is small and the boundary condition can only be satisfied if the term following $(1+R)$ is zero. After changing spatial variables, $n \to x$ and $\sigma \to y$, we arrive at the modified equation model corresponding to the discrete half-plane problem (50)-(51) in domains where the normal is not aligned with the mesh:

$$u_{tt} = u_{xx} + u_{yy} - \alpha h^3 u_{tyyyy}, \quad \alpha \geq 0, \quad x \geq 0, \quad -\infty < y < \infty, \tag{58}$$

$$u_x = \beta_1 h^4 u_{yyyyy} + \beta_2 h^3 u_{yyyy}, \quad x = 0, \quad |u| \leq \text{const.} \tag{59}$$

We have added a dissipation term to the differential equation because we shall need it later. Note that we have only added dissipation in the tangential direction, to avoid having to add any extra boundary conditions.

After Fourier transforming in y and Laplace transforming in t we obtain

$$\hat{u}_{xx} = (s^2 + \omega^2)\hat{u} + sa\hat{u}, \quad a = \alpha h^3 \omega^4, \quad \text{Re } s > 0, \tag{60}$$

with boundary conditions

$$\hat{u}_x(0) = b\hat{u}(0), \quad |\hat{u}| \leq \text{ const. }, \quad b = i\beta_1 \omega^5 h^4 + \beta_2 \omega^4 h^3. \tag{61}$$

As $|\omega|$ becomes larger, the Fourier symbol of the second divided difference, $-\frac{4}{h^2}\sin^2\left(\frac{\omega h}{2}\right)$, deviates more and more from the Fourier symbol of a second derivative, $-\omega^2$. In particular, for the highest frequency on the mesh ($\omega h = \pi$), the symbol of the second divided difference is $-4/h^2$, while the symbol of the second derivative is $-\pi^2/h^2$. Hence, the highest frequencies on the mesh are not accurately modeled by the modified equation. We therefore restrict the following analysis to $|\omega h| \leq 1$.

The general solution of (60) is given by

$$\hat{u} = \sigma_1 e^{\lambda x} + \sigma_2 e^{-\lambda x}, \tag{62}$$

where λ now satisfies

$$\lambda = \sqrt{s^2 + \omega^2 + sa}, \quad \text{Re}\,\lambda \geq 0. \tag{63}$$

Since $\text{Re}\,\lambda > 0$ for $\text{Re}\,s > 0$, the boundary conditions are satisfied if and only if

$$\sigma_1 = 0, \quad \lambda = -b = -(i\beta_1 \omega^5 h^4 + \beta_2 \omega^4 h^3). \tag{64}$$

There are two possibilities:

1. If $\beta_2 \geq 0$, then there are no solutions of (64) with $\text{Re } s > 0$ since $\text{Re}\,\lambda > 0$, but $\text{Re}\,(-b) \leq 0$. Furthermore, when the dissipation coefficient $\alpha > 0$, $\text{Re}\,\lambda > 0$ also for $\text{Re}\,s = 0$, $\omega \neq 0$. Hence, there are no generalized eigenvalues when $\alpha > 0$ and we conclude that the half-plane problem is stable.

2. If $\beta_2 < 0$, then the problem can be unstable. We want to show that if $|\beta_1|$ and $|\beta_2|$ are small, the problem can be stabilized by a small $\alpha > 0$.

Theorem 3 *If $\beta_2 < 0$, $|\beta_2| \ll 1, |\beta_1| \ll 1$ and $\alpha \geq K|\beta_1\beta_2|$, $K = const.$, the modified half-plane problem (58)-(59) is stable, i.e., the eigenvalue problem (60)-(61) has no solutions with $Re\, s > 0$ and no generalized eigenvalues $Re\, s = 0$ for $\omega \neq 0$.*

Proof. Introducing (64) into (63) gives

$$s^2 + sa + \omega^2 - b^2 = 0.$$

Since $|\omega h| \leq 1$, $|a| \leq |\alpha||\omega|$. If we assume $0 \leq \alpha \leq 1$, we have $|a| \leq |\omega|$ and $\omega^2 - a^2/4 \geq 3\omega^2/4$. Therefore,

$$s = -\frac{a}{2} \pm i\sqrt{\left(\omega^2 - \frac{a^2}{4}\right)}\sqrt{1 - \frac{b^2}{\omega^2 - a^2/4}}. \tag{65}$$

By assumption $|b^2| \ll \omega^2$. We can therefore expand the square root and conclude that

$$s = -\frac{a}{2} \pm \left(i\sqrt{\left(\omega^2 - \frac{a^2}{4}\right)} - \frac{ib^2}{2\sqrt{\omega^2 - a^2/4}} + \dots\right).$$

Hence,

$$\text{Re } s \approx -\frac{\alpha}{2}h^3\omega^4 \pm \frac{\text{Im } b^2}{2\sqrt{\omega^2 - a^2/4}} = -\frac{\alpha}{2}h^3\omega^4 \pm \frac{\beta_1\beta_2(\omega h)^7\omega^2}{\sqrt{\omega^2 - a^2/4}} < 0$$

for $\alpha \geq 4|\beta_1\beta_2|/\sqrt{3}$.

We have numerically computed the truncation error coefficients β_1 and β_2 for our boundary condition approximation. To conserve space, we will only report the result of these computations here. For all possible directions of the boundary normal and all permissible distances between the ghost point and the boundary, we found that $-0.065 < \beta_2 < 0.015$ and $-0.063 < \beta_1 < 0.063$. It is critical that $|\beta_2|$ is small since the case $\beta_2 < 0, |\beta_2| = \mathcal{O}(1)$ can not be stabilized by adding a dissipative term to the differential equation. In earlier versions of our numerical code we added a tangential smoothing operator to the boundary condition approximation. In terms of the modified problem this means that $\beta_2 > 0$. The dissipation operator proposed in Section 1 seems to be so efficient that this extra smoothing operator is not needed.

6 The two-dimensional strip problem

We here generalize the modified equation approach to study the stability of solutions on a bounded domain,

$$u_{tt} = u_{xx} + u_{yy} - \alpha h^3 u_{tyyyy}, \quad \alpha \geq 0, \quad 0 \leq x \leq 1, \quad -\infty < y < \infty, \tag{66}$$

$$u_x = \beta_1 h^4 u_{yyyyy} + \beta_2 h^3 u_{yyyy}, \; x = 0, \quad u_x = 0, \; x = 1. \tag{67}$$

Remark: In reality the boundary condition at $x = 1$ also contains truncation order terms, but the results are the same.

After Fourier and Laplace transforming the problem, (66)-(67) becomes

$$s^2\hat{u} = \hat{u}_{xx} - (\omega^2 + as)\hat{u}, \quad a = \alpha h^3\omega^4, \tag{68}$$

$$\hat{u}_x(0) = b\hat{u}(0),\ \hat{u}_x(1) = 0, \quad b = i\beta_1\omega^5 h^4 + \beta_2\omega^4 h^3. \tag{69}$$

The general solution of (68) now has the form

$$\hat{u} = \sigma_1 e^{\lambda x} + \sigma_2 e^{-\lambda x} \tag{70}$$

where λ is the solution of (63), i.e., $\mathrm{Re}\,\lambda > 0$ for $\mathrm{Re}\ s > 0$. Introducing (70) into (69) shows that there is a nontrivial solution if and only if

$$\frac{\lambda - b}{\lambda + b} = e^{2\lambda}. \tag{71}$$

We have already studied the corresponding half-plane problem and shown that for $\beta_2 \geq 0$, there are no eigenvalues s, with $\mathrm{Re}\,s > 0$ and that there are no generalized eigenvalues when $\alpha > 0$. For $\beta_2 < 0$, Theorem 3 shows when the half-plane problem is stable. Hence, it can be expected that the strip problem also is stable. In Appendix B, we perform a detailed calculation to verify the stability of the strip problem. From this calculation, we can also read off the order of magnitude of the dissipation coefficient α that is necessary for stability. The results are summarized in

Theorem 4 *If the half-plane problem (58) - (59) is stable, the modified strip problem (66) - (67) is stable for $\alpha > 0$, $\alpha = \mathcal{O}(h^{3/4})$.*

7 General two-dimensional domains

In this section, we will add some details to our proposed scheme that were left out from the general description in Section 1.

7.1 Near boundary behavior of the discretized Laplacian

The discretized Neumann boundary condition (3) can be used to eliminate all ghost point values in the discretized Laplacian (2). Referring to the case shown in Figure 1, we get at the point $(i, j+1)$,

$$\begin{aligned}\Delta_h v^n_{i,j+1} = \frac{1}{h^2}(v^n_{i+1,j+1} + v^n_{i-1,j+1} + v^n_{i,j+2} - 4v^n_{i,j+1}) - \\ \frac{g_I}{h^2 g_0}(c_0 v^n_{i,j+1} + c_1 v^n_{i+1,j+1} + c_2 v^n_{i+2,j+1}) - \\ \frac{g_{II}}{h^2 g_0}(c_3 v^n_{i,j+2} + c_4 v^n_{i+1,j+2} + c_5 v^n_{i+2,j+2}) + \frac{f(\boldsymbol{x}^\Gamma_{i,j}, t_n)}{h^2 g_0},\end{aligned} \tag{72}$$

N	$\|\boldsymbol{e}^I\|_\infty$	$\|h^3 A^T \boldsymbol{u}\|_\infty$	h
171	3.43×10^{-4}	4.36×10^{-2}	2.82×10^{-2}
341	9.21×10^{-5}	2.20×10^{-2}	1.41×10^{-2}
681	2.40×10^{-5}	1.20×10^{-2}	7.06×10^{-3}

Table 1: Smoothing properties of the operator A investigated by solving $A\boldsymbol{e}^I = h^3 A^T \boldsymbol{u}$ for different grid sizes for the case shown in Figure 2. Clearly, $\boldsymbol{e}^I = \mathcal{O}(h^2)$ while $h^3 A^T \boldsymbol{u} = \mathcal{O}(h)$.

assuming that (i, j) is the only nearest neighbor of $(i, j+1)$ that is outside of Ω. If additional points are outside, other formulas of the type (3) would be used to eliminate those points as well. The coefficients g_0, g_I, g_{II} are given by (4). Since $0 \leq \xi_\Gamma \leq \xi_I$ and $h \leq \xi_I \leq \sqrt{2}h$, the denominator g_0 satisfies

$$\frac{1}{2\sqrt{2}h} \leq \frac{1}{2\xi_I} \leq |g_0| \leq \frac{3}{2\xi_I} \leq \frac{3}{2h}.$$

Because the coefficient g_0 in (72) is bounded away from zero, we conclude that this discretization of the Laplacian does *not* suffer from "small cell" stiffness problem.

7.2 Accuracy of the damped scheme

For simplicity, let the grid function $\boldsymbol{v}$ satisfy the semi-discrete problem, where time is left continuous,

$$\boldsymbol{v}_{tt} = A\boldsymbol{v} + \boldsymbol{b} + \boldsymbol{F} - \alpha h^3 A^T \left(A\boldsymbol{v}_t + \boldsymbol{b}_t\right),$$

Let the error in the discrete solution be $\boldsymbol{e} = u - \boldsymbol{v}$, where u is the solution of the continuous problem (1) evaluated on the grid. We have

$$\begin{aligned} \boldsymbol{e}_{tt} &= \Delta u - A\boldsymbol{v} - \boldsymbol{b} + \alpha h^3 A^T \left(A(\boldsymbol{v}_t + u_t - u_t) + \boldsymbol{b}_t\right). \\ &= \Delta u - Au - \boldsymbol{b} + A\boldsymbol{e} - \alpha h^3 A^T A\boldsymbol{e}_t + \alpha h^3 A^T \left(Au_t + \boldsymbol{b}_t\right). \end{aligned}$$

We split the error according to $\boldsymbol{e} = \boldsymbol{e}^I + \boldsymbol{e}^{II}$ and let $\boldsymbol{e}^I$ satisfy

$$A\boldsymbol{e}^I = -\alpha h^3 A^T \left(Au_t + \boldsymbol{b}_t\right). \tag{73}$$

Now, $Au_t + \boldsymbol{b}_t$ is a second order accurate approximation of Δu_t evaluated on the grid. Furthermore, away from the boundary, $A^T \Delta u_t$ is a second order approximation of $\Delta^2 u_t$, but near the boundary $A^T \Delta u_t = \mathcal{O}(\Delta u_t / h^2)$. Hence the right hand side of (73) is $\mathcal{O}(h)$ near the boundary but $\mathcal{O}(h^3)$ in the interior. Due to the smoothing properties of the elliptic operator A (see figure 2 and table 1 for a numerical example), we gain one order of magnitude when solving for $\boldsymbol{e}^I$, resulting in

$$\boldsymbol{e}^I = \mathcal{O}(h^2).$$

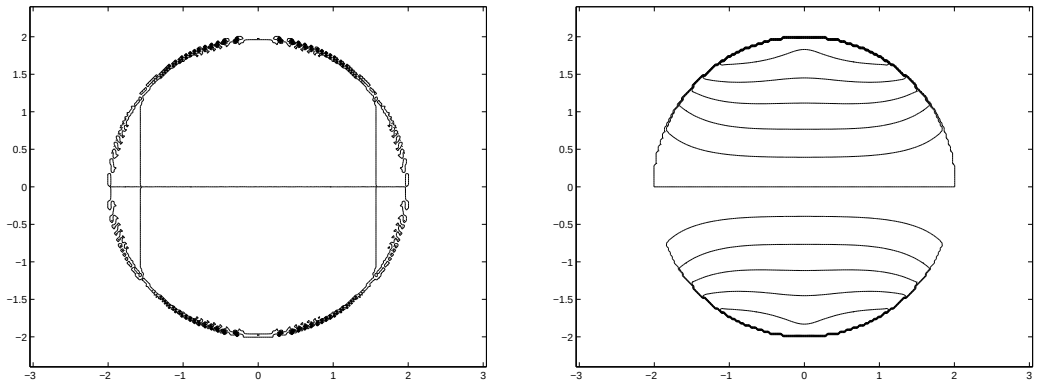

Figure 2: Numerical test of the smoothing properties of $A\boldsymbol{e}^I = h^3 A^T \boldsymbol{u}$. The left figure shows a contour plot of the right hand side $h^3 A^T \boldsymbol{u}$ and the right figure shows the solution $\boldsymbol{e}^I$ for $N = 171$, see Table 1 for quantitative information. In this case, the computational domain was a circle with unit radius and the test function was $\boldsymbol{u}_{i,j} = \cos(x_i)\sin(y_j)$. The problem was solved using the conjugated gradient algorithm.

Since the right hand side of (73) is smooth in time, we also have $\boldsymbol{e}^I_{tt} = \mathcal{O}(h^2)$ and $A\boldsymbol{e}^I_t = \mathcal{O}(h)$. The equation for $\boldsymbol{e}^{II}$ is

$$\boldsymbol{e}^{II}_{tt} = A\boldsymbol{e}^{II} - \alpha h^3 A^T A \boldsymbol{e}^{II}_t - \boldsymbol{e}^I_{tt} - \alpha h^3 A^T A \boldsymbol{e}^I_t + \Delta u - (Au + \boldsymbol{b}).$$

Because $Au + \boldsymbol{b}$ is a second order accurate approximation of Δu and $h^3 A^T A \boldsymbol{e}^I_t = \mathcal{O}(h^2)$, all forcing terms are of the order $\mathcal{O}(h^2)$. Hence

$$\boldsymbol{e}^{II} = \mathcal{O}(h^2),$$

which shows that the damped scheme is second order accurate.

7.3 Fourth order corrections

To reduce the phase-error away from the boundary, we can optionally add a fourth order correction term

$$\Delta_{h,4} v^n_{i,j} = -\frac{h^2}{12}\left(D^x_+ D^x_- \gamma_{i,j} D^x_+ D^x_- + D^y_+ D^y_- \gamma_{i,j} D^y_+ D^y_-\right) v^n_{i,j},$$

to our second order accurate approximation of the Laplacian. Clearly, this stencil is too wide to be evaluated all the way up to the boundary, so the grid function $\gamma_{i,j}$ must be identically zero in a band near the boundary. Away from the boundary we want $\gamma_{i,j} \equiv 1$ to make the correction term cancel the second order truncation error in $\Delta_h v_{i,j}$. To aid in the construction of $\gamma_{i,j}$, we initially compute a smoothed distance function $d_{i,j} \geq 0$ using the technique described in [16]. The value of the distance function at a grid point approximately equals the distance between that grid point and the nearest boundary. Hence, the distance function is zero on the boundary and increases monotonically away

from the boundary, making it straight forward to construct a smooth $\gamma_{i,j}$ that is zero near the boundary ($d_{i,j} \leq \epsilon_1$) and one away from the boundary ($d_{i,j} \geq \epsilon_2$). In all numerical examples presented below, we used $\epsilon_1 = 3h$ and $\epsilon_2 = 13h$. The resulting scheme can be written in semi-discrete form as

$$\boldsymbol{v}_{tt} = A\boldsymbol{v} + B\boldsymbol{v} + \boldsymbol{F} + \boldsymbol{b} - \alpha h^3 A^T \left(A\boldsymbol{v}_t + \frac{d\boldsymbol{b}}{dt}(t_n) \right), \tag{74}$$

where B represent the fourth order correction term. The symmetry of B and the smoothness of the distance function of $\gamma_{i,j}$ seems to give stability. A heuristic argument for this is that B can not generate any boundary layer instability, since this type of instability decays rapidly away from the boundary and in this region $\Delta_{h,4} v^n_{i,j}$ is arbitrary small. And the other type of instability discussed above, highly oscillatory in the whole domain, is effectively stabilized by our damping term. The smoothness of the distance function imply that no new spurious solutions are generated. The smoothness furthermore guarantees accuracy of order two in the transition region. Hence, the resulting scheme will only be second order accurate. The main benefit of the fourth order spatial correction will be a reduced phase error away from the boundary. For this reason we will call the resulting scheme the "internally fourth order" method.

We can also improve the basic second order time-integration method by using a fourth order accurate Taylor series method. Consider the second order system of ODE's

$$\boldsymbol{w}_{tt} = C\boldsymbol{w} + \boldsymbol{F},$$

where C is a symmetric negative semi-definite matrix. A fourth order time-discretization is given by

$$\frac{\boldsymbol{w}^{n+1} - 2\boldsymbol{w}^n + \boldsymbol{w}^{n-1}}{k^2} = C\boldsymbol{w}^n + \boldsymbol{F}^n + \frac{k^2}{12}\left(C(C\boldsymbol{w}^n + \boldsymbol{F}^n) + \boldsymbol{F}^n_{tt} \right), \tag{75}$$

and it is stable for

$$\max_j(-\lambda_j)k^2 < 12,$$

where λ_j are the real-valued non-positive eigenvalues of C. The scheme (75) can be formulated in predictor-corrector form,

$$\tilde{\boldsymbol{w}}^{n+1} = 2\boldsymbol{w}^n - \boldsymbol{w}^{n-1} + k^2 C\boldsymbol{w}^n + k^2\boldsymbol{F}^n, \tag{76}$$

$$\boldsymbol{w}^{n+1} = \tilde{\boldsymbol{w}}^{n+1} + \frac{k^2}{12}\left(C(\tilde{\boldsymbol{w}}^{n+1} - 2\boldsymbol{w}^n + \boldsymbol{w}^{n-1}) + k^2\boldsymbol{F}^n_{tt} \right). \tag{77}$$

Hence, the predictor step (76) is simply the second order time-integration scheme presented above. The discrete damping term is added to the predictor-corrector scheme in the same way as in (6). For the spatially fourth order method, we take $C = A + B$, otherwise $C = A$. We note that the corrector step (77) needs only a second order accurate

approximation of $\boldsymbol{w}_{tt}$. Hence, from an accuracy standpoint we can omit the damping term and always take $C = A$ in this step. Numerical experiments, see Section 8, indicate that the resulting scheme is stable.

We start the time-integration at $n = 0$. For the fourth order time-discretization, we take $v^0_{i,j} = u_0(x_i, y_j)$ and need to use a fifth order accurate approximation of $u(x_i, y_j, -k)$ for $v^{-1}_{i,j}$. This is achieved by using the differential equation to approximate higher order time derivatives,

$$\begin{aligned} v^{-1}_{i,j} = u_0(x_i,y_j) - ku_1(x_i,y_j) + \frac{k^2}{2}\left(D^x_+D^x_- + D^y_+D^y_-\right)u_0(x_i,y_j) + \frac{k^2}{2}F(\boldsymbol{x}_{i,j},0) \\ - \frac{k^3}{6}(D^x_+D^x_- + D^y_+D^y_-)u_1(x_i,y_j) - \frac{k^3}{6}F_t(\boldsymbol{x}_{i,j},0) \\ - \frac{k^2h^2}{24}\left((D^x_+D^x_-)^2 - (D^y_+D^y_-)^2\right)u_0(x_i,y_j) \\ + \frac{k^4}{24}(D^x_+D^x_- + D^y_+D^y_-)^2u_0(x_i,y_j) + \frac{k^4}{24}F_{tt}(\boldsymbol{x}_{i,j},0). \end{aligned} \tag{78}$$

Note that the last three lines can be omitted for the second order time-discretization.

8 Numerical examples

In this section we numerically solve (1) with the schemes described above. For the cases where an analytical solution is known, we use this solution to initialize the computation at time levels $t = -k$ and $t = 0$. For the cases where an analytical solution is not known we use the initialization (78).

We will denote the CFL-number by $\text{CFL} \equiv k/h$. Note that for a two-dimensional periodic domain, our second order time-integration scheme (6) is stable for $\text{CFL} \leq 1/\sqrt{2} \approx 0.71$ while the fourth order predictor-corrector scheme (76),(77) is stable for $\text{CFL} \leq \sqrt{3/2} \approx 1.22$. Also note that all errors are measured in max-norm.

In all examples presented below, the fourth order predictor-corrector time-integrator (76),(77) is used together with the internally fourth order spatial correction. The second order scheme (6) is always used together with the second order spatial discretization. Unless otherwise noted, the Neumann boundary condition is discretized using the third order accurate formula to reduce the constant in the second order truncation error, as was mentioned in the introduction.

To evaluate the accuracy of the method, the forcing functions is chosen such that the exact solution is the trigonometric traveling wave:

$$u(x,y,t) = \sin(\omega(x-t))\sin(\omega y), \quad \omega = 4\pi. \tag{79}$$

The domain Ω is taken to be an ellipse centered at the origin with semi-axes $x_s = 1$ and $y_s = 0.75$. The Cartesian grid covers the rectangle $-1.1 \leq x \leq 1.1$, $-0.85 \leq y \leq 0.85$.

		2'nd order scheme			Predictor-corrector scheme		
t	α	$N = 101$	$N = 201$	ratio	$N = 101$	$N = 201$	ratio
2.0	0.0	8.75e-02	2.10e-02	4.17	10.7e-02	2.17e-02	4.93
2.0	0.001	8.77e-02	2.10e-02	4.18	10.7e-02	2.17e-02	4.93

Table 2: Grid refinement study showing the errors in the computed solutions when the exact solution is the trigonometric function (79). Here, CFL=0.5 for the second order scheme and CFL=1.0 for the internally fourth order predictor-corrector scheme. The grid size $N = 101$ corresponds to $h = 2.4 \times 10^{-2}$ and $N = 201$ corresponds to $h = 1.2 \times 10^{-2}$. The first line corresponds to the undamped case, $\alpha = 0$ and the second line shows the damped case with $\alpha = 0.001$.

In Table 2, we present a grid refinement study for the second order scheme (6) and the internally fourth order predictor-corrector scheme (76),(77). The fourth order correction only applies in the interior of the domain, and the second order errors near the boundary clearly dominates the total error. Hence, in this case, there is no apparent benefit of using the internally fourth order method. The time step can be taken twice as large, but this gain is balanced by having to evaluate the Laplacian twice instead of once per time step. Also note that the influence of the damping term is so small that it only changes the last digit in the error in one of these runs.

To more clearly illustrate the benefits of using a fourth order correction away from the boundary, we select the forcing function F and boundary data f such that the exact solution is a spatially localized, outwardly traveling wave,

$$u(x, y, t) = \phi(\sqrt{x^2 + y^2} - t), \quad \phi(\xi) = \frac{1}{2}\left(1 + \tanh\frac{\xi - \xi_0}{\epsilon}\right)\left(1 - \tanh\frac{\xi - \xi_1}{\epsilon}\right). \quad (80)$$

Note that such waves are exact solutions to the unforced wave equation in one and three space dimensions, but not in the two-dimensional case. The domain Ω is taken to be the circle, $|r| \leq 1.5$, and the Cartesian grid covers the square $-1.6 \leq x \leq 1.6$, $-1.6 \leq y \leq 1.6$. The parameters in ϕ are taken to be

$$\xi_0 = 0.3, \quad \xi_1 = 0.5, \quad \epsilon = 0.07.$$

The wave reaches the boundary at $t \approx 0.8$. In Table 3 we see that for the internally fourth order method, the error is at least one order of magnitude smaller and the convergence rate is much higher before the wave hits the boundary. No such distinction can be made for the second order method, where the errors grow more gradually in time. Furthermore, the errors in the internally fourth order method are substantially smaller than those of the second order method, especially before the wave hits the boundary.

We proceed by investigating the long time stability properties of the method. We take the domain to be the same ellipse used above, and take the forcing functions such that

	2'nd order scheme			Predictor-corrector scheme		
t	$N = 201$	$N = 401$	ratio	$N = 201$	$N = 401$	ratio
0.5	3.29e-2	8.63e-3	3.8	1.23e-3	8.78e-5	14.0
0.75	4.59e-2	1.23e-2	3.7	1.73e-3	1.26e-4	13.7
1.0	1.05e-1	3.12e-2	3.4	2.71e-2	3.23e-3	8.4
1.25	5.89e-2	1.73e-2	3.4	1.76e-2	2.53e-3	6.9

Table 3: Grid refinement study showing the errors in the computed solutions when the exact solution is the outwardly traveling wave function (80). Here, CFL=0.5 for the second order scheme and CFL=1.0 for the predictor-corrector scheme. The grid size $N = 201$ corresponds to $h = 1.8 \times 10^{-2}$ and $N = 401$ corresponds to $h = 9.0 \times 10^{-3}$. In all cases, the damping coefficient was $\alpha = 10^{-3}$.

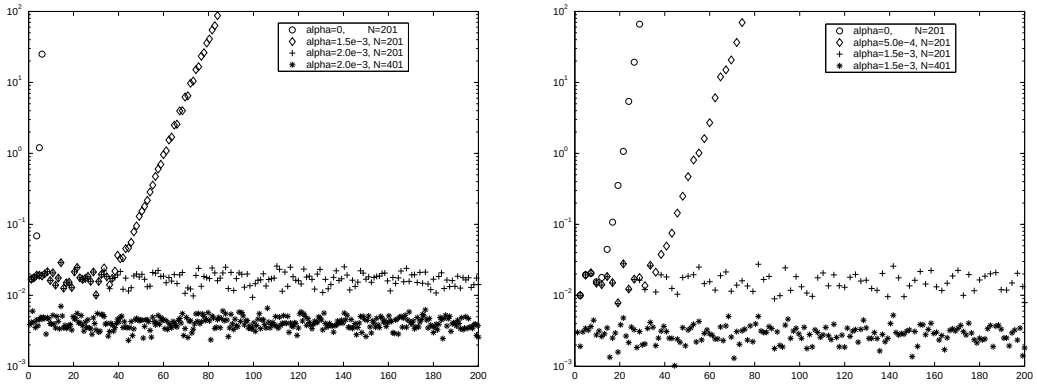

Figure 3: The max norm of the error in the solution as function of time. The second order scheme (6) was run at CFL=0.5 (left), and the predictor-corrector method (76),(77) was run at CFL=1.0 (right). Note that to stabilize the solution, the damping coefficient had to be slightly larger for the second order scheme (2×10^{-3}) than the predictor-corrector method (1.5×10^{-3}).

the exact solution is the trigonometric traveling wave (79). In Figure 3, we show the error in the solution as function of time, for different values of α and for different grid sizes. We conclude that it is sufficient to take $\alpha = 2 \times 10^{-3}$ for both the second order and the predictor-corrector scheme. Note that these computations integrated the solution for long times. In particular, the second order scheme on the finer grid ($N = 401$) required 66,666 time steps to reach $t = 200$. Also note that there is no long-time increase in the error, which indicates that the damping is very mild.

We next study the homogeneous problem

$$F(\boldsymbol{x}, t) \equiv 0, \quad f(\boldsymbol{x}, t) \equiv 0,$$

in a domain bounded by an ellipse centered at the origin, with semi-axes $x_s = 2.0$ and $y_s = 2.54$. The Cartesian grid covers the square $-2.1 \le x \le 2.1$, $-2.64 \le y \le 2.64$. We

take initial data to be

$$u_0(x,y) = \phi(\sqrt{x^2 + (y - y_F)^2}),$$

where $\phi(\xi)$ is given by (80). The upper focal point is located at $y_F = \sqrt{y_s^2 - x_s^2} \approx 1.56$ and

$$u_1(\boldsymbol{x}) = -\phi'(\sqrt{x^2 + (y - y_F)^2}).$$

The parameters in $\phi(\xi)$ are

$$\xi_0 = 0.2, \quad \xi_1 = 0.4, \quad \epsilon = 0.035.$$

Note that the initial data is chosen such that the wave is essentially traveling radially outwardly from the focal point $(0, y_F)$. By making a ray-tracing argument, we see that a high frequency wave should reflect the boundary and re-focus at the other focal point $(0, -y_F)$. This was verified for the Dirichlet problem in [2] (Figure 6). For the Neumann boundary condition, we should get a similar behavior, except that the solution should have the opposite phase compared to the Dirichlet case. This is confirmed in Figure 4, where we show a well-resolved calculation using the predictor-corrector scheme with $N = 801$ and CFL=1.0. It is interesting to use this calculation as a yard-stick to compare the quality of the solutions from both schemes at a lower resolution, $N = 401$, see Figure 5 and 6. Observe the more pronounced over and undershoots for the second order method in comparison to the predictor-corrector method, indicating that the phase-error dominates at the time of comparison. In all these calculations, the damping coefficient was $\alpha = 0.001$.

While all theory and all numerical experiments up to this point have been presented for the third order accurate discretization of the boundary conditions, our practical experience with the second order boundary condition stencil is at least as good. The advantage of the second order stencil is that it uses fewer internal points, which becomes important for thin or marginally resolved geometries. However, near true corners, the second order boundary condition needs to be modified to avoid using grid points where the solution is undefined, see Figure 7. To avoid this problem, all grid points are first scanned in a preprocessing step to detect interior points within $\sqrt{2}h$ of corners. All such points that also have at least two exterior nearest neighbors, get marked with a '-1'. The boundary condition stencil at ghost points neighboring a '-1' point is then modified to be a divided difference between the ghost point and the '-1' point, i.e., the direction of the normal is locally changed to be either vertical or horizontal. As a consequence, no undefined points are involved in the boundary stencil near the corner and the resulting contribution to the discretized Laplace operator (the matrix A) will be locally symmetric.

While the modified boundary condition approximation will be at most first order accurate near each corner, it is not clear what impact that truncation error has on the accuracy of the solution. We are also interested in the long-time stability of the resulting scheme. To investigate these issues, we take the domain to be a square with side length 2, rotated 10 degrees relative to the grid directions. In rotated coordinates $\tilde{x} = x\cos(\theta) +$

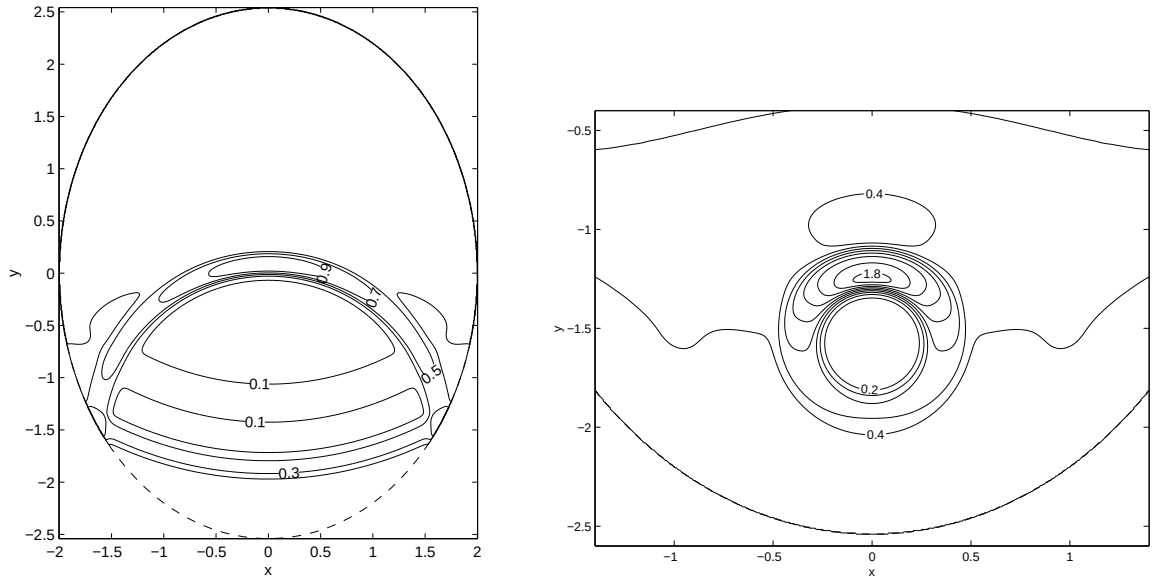

Figure 4: Contours of the bouncing wave solution to the Neumann problem. Here a reference solution is produced with the predictor-corrector scheme, CFL=1.0, $N = 801$, $t = 3.12$(left) and $t = 4.41$(right). The dashed line is the boundary and the contour spacing is 0.2.

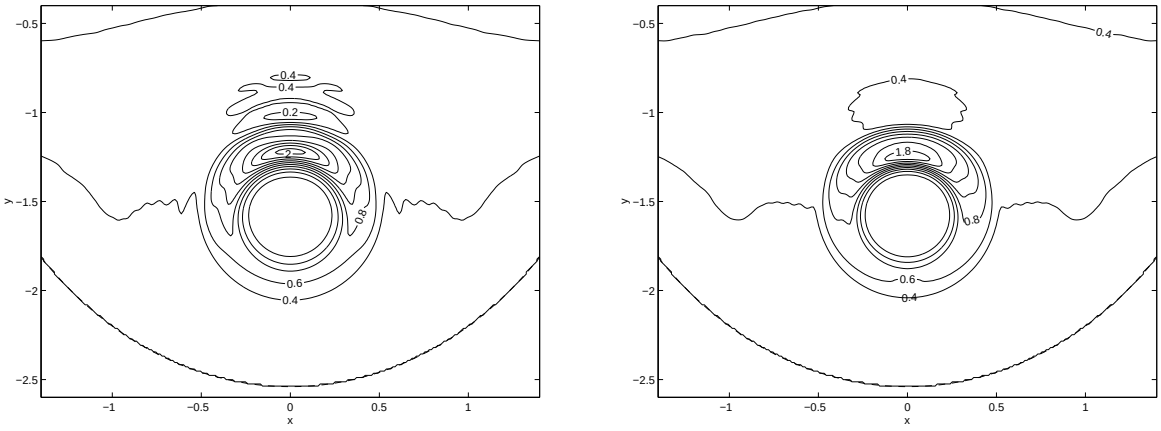

Figure 5: Contours of the bouncing wave solution to the Neumann problem. The second order scheme is used with CFL= 0.5(left) and the predictor-corrector scheme is used with CFL= 1.0(right). Here $N = 401$, $t = 4.41$, and the contour spacing is 0.2.

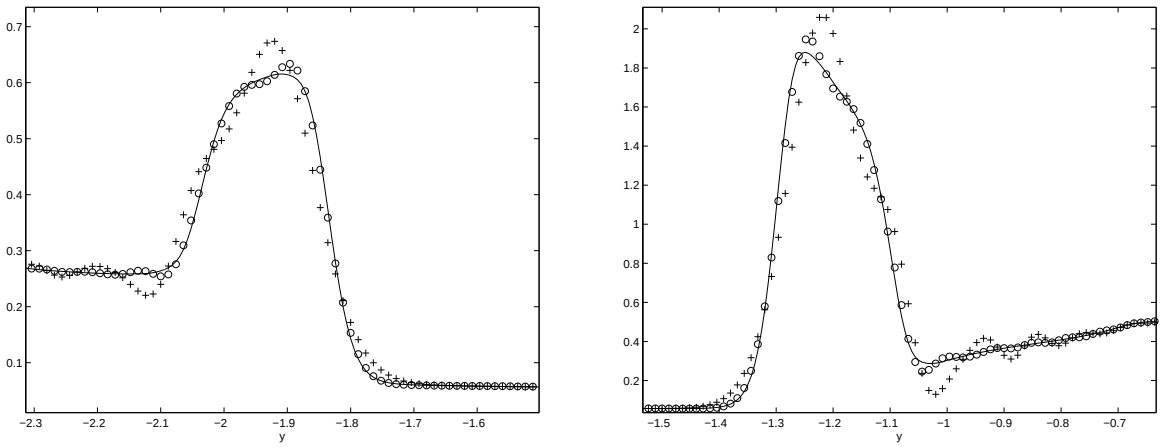

Figure 6: Comparison of the bouncing wave solution for the Neumann problem at $t = 4.41$ along the line $x = 0$ centered around $y = -2.0$(left) and $y = -1.2$(right). The reference solution is for $N = 801$(solid), the second order scheme is for $N = 401$, CFL=0.5('+') and the predictor-corrector scheme is for $N = 401$, CFL=1.0('o').

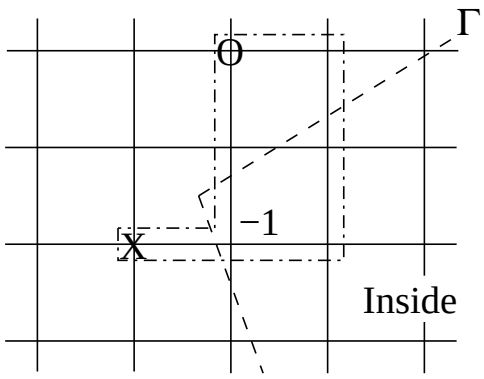

Figure 7: The standard second order boundary condition stencil (outlined with a dash-dotted line) for the ghost point at 'X' involves the point 'O', where the solution is undefined due to the corner. In this case, the boundary stencil at 'X' is reduced to a divided difference between the solution at '-1' and 'X'.

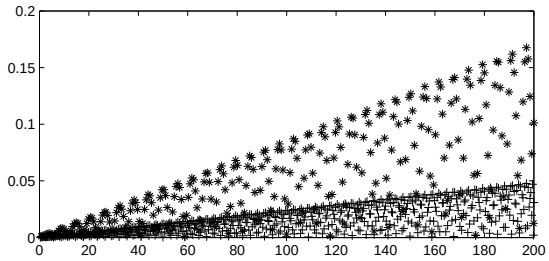

Figure 8: The max norm of the error for a rotated square domain, as function of time. The '*' correspond to the grid size $h = 1.417 \times 10^{-2}$, and '+' represent the grid size $h = 7.087 \times 10^{-3}$. The damping coefficient was $\alpha = 2 \times 10^{-3}$.

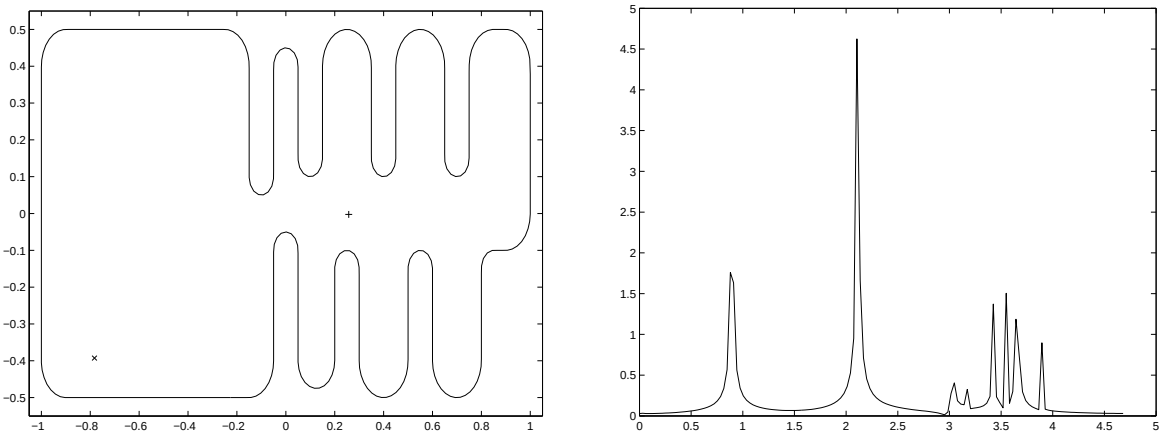

Figure 9: The geometry for the harbor model (left). The computational grid covered $-1.05 \leq x \leq 1.05$, $-0.55 \leq y \leq 0.55$ and had 801×401 grid points corresponding to the grid size $h = 2.6 \times 10^{-3}$. The forcing is located at the 'x' and the signal is recorded at the '+'. The right figure shows the lowest modes in the discrete Fourier transform of the recorded signal, as function of the frequency. The spikes indicate eigenfrequencies.

$y\sin(\theta)$, $\tilde{y} = -x\sin(\theta) + y\cos(\theta)$, $\theta = 10\pi/180$, an exact solution of the homogeneous wave equation can be constructed using Fourier expansion. Here we take

$$u(\tilde{x}, \tilde{y}, t) = \sin\left(\frac{\pi\tilde{x}}{2}\right)\sin\left(\frac{3\pi\tilde{y}}{2}\right)\cos(\omega t), \quad \omega = \frac{\pi\sqrt{10}}{2},$$

which satisfies homogeneous Neumann conditions along $\tilde{x} = \pm 1$ and $\tilde{y} = \pm 1$, respectively. The errors in the computed solutions on two grid sizes are reported in Figure 8, indicating that the solution is almost second order accurate despite the corners. However, for reasons not currently understood, the errors accumulate and seem to grow linearly in time.

In our last numerical example, we use the numerical method to compute the eigenfrequencies and eigenmodes of the domain shown i Figure 9. Since the wave equation models the propagation of small amplitude water waves, we may think of this geometry as representing a simple harbor. Even though the grid is rather fine, the wide stencil used by the third order boundary condition couples the solution at some ghost points near the ends of the convex fingers protruding into the domain. By coupling we mean that at least one of the interior points in one boundary condition stencil is also a ghost point. Satisfying the boundary conditions at all ghost points would then require an iteration over the ghost point values. To avoid this iterative procedure, we will instead use the second order boundary condition, which uses fewer interior points in its stencil. For this case, the solution does not get coupled at any ghost points. To estimate the eigenfrequencies,

we apply a forcing to two consecutive points in space,

$$F(x_{i,j}, y_{i,j}, t) = \begin{cases} Ke^{-(t-t_0)^2/\varepsilon_1^2}, & i = I_1, j = J_1, \\ -Ke^{-(t-t_0)^2/\varepsilon_1^2}, & i = I_1 + 1, j = J_1, \\ 0, & \text{otherwise.} \end{cases}$$

Here $K = 10^5$, $\varepsilon_1 = 0.07$, $t_0 = 1.0$. We choose this forcing since it is likely to have a component along each eigenmode, except the constant mode corresponding to the zero eigenvalue, which is present due to the Neumann boundary condition. We start the computation from rest and integrate up to time $T = 200$. During the computation, the solution is recorded at another point (I_r, J_r). This signal is then Fourier transformed in time, after which the eigenfrequencies of the domain appear as spikes in the spectrum, see Figure 9. Note that the frequency resolution is limited by $2\pi/T$, so a longer computation leads to a more accurate estimate of the eigenfrequencies. Also note that the eigenvalues of

$$\begin{aligned} \Delta u &= \lambda u, \quad \text{in } \Omega, \\ \frac{\partial u}{\partial n} &= 0, \quad \text{on } \Gamma, \end{aligned}$$

are related to the eigenfrequencies ω through $\lambda = -\omega^2$.

To compute the corresponding eigenmode, we perform a second computation, where the forcing is taken to be

$$F(x, y, t) = \sin(\omega_r t)\gamma'(x - x_0)\gamma(y), \qquad \gamma(\xi) = e^{-\xi^2/\varepsilon_2^2}, \quad x_0 = -0.6, \ \varepsilon_2 = 0.2.$$

The frequency of the time-harmonic forcing is chosen to obtain resonance. In this computation, we take $\omega_r = 0.90$, which is the approximate location of the first spike in the spectrum, see Figure 9. Due to resonance, the solution will be more and more dominated by the corresponding eigenmode as time increases, assuming that the forcing is not orthogonal to that mode. The resulting eigenmode is shown in Figure 10 together with the time-history of the solution in one point, which demonstrates the expected linear growth in amplitude.

9 Conclusions

We have presented stability theory and numerical examples for a Cartesian embedded boundary scheme that directly discretizes the second order wave equation subject to Neumann boundary conditions, without rewriting the problem as a system of first order equations. Since the discrete approximation of the Laplacian subject to the Neumann

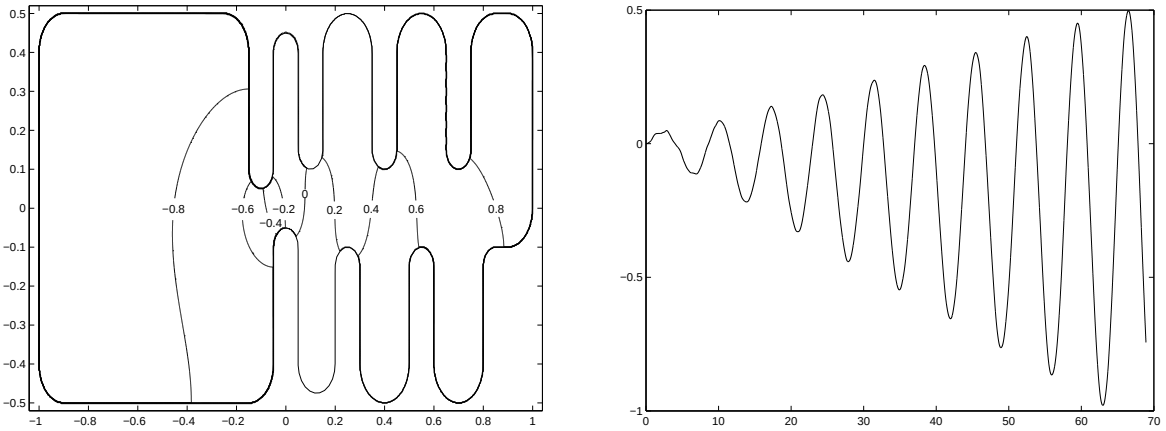

Figure 10: A contour plot of the solution at $t = 62.4$ approximating the eigenmode corresponding to the eigenfrequency $\omega_r = 0.90$ (left). Here, the contour levels are equally spaced between -0.8 and 0.8. The right figure shows the time-history of the solution at the point $(x, y) = (-0.6526, -0.1976)$. Because of resonance, the amplitude grows linearly in time.

boundary condition leads to a matrix A that is not symmetric, the stability theory developed in [2] does not directly apply. Indeed, numerical experiments in two-dimensional domains indicate that the basic un-damped scheme is unstable. In the one-dimensional case, we prove that the semi-discrete scheme is stable, thus indicating that the instability is due to two-dimensional effects. In two dimensions, tangential derivatives are present in the truncation error of the boundary condition, when the boundary is not aligned with the mesh. A two-dimensional stability theory is presented that first is used to show the de-stabilizing effect of perturbing a Neumann boundary condition by tangential derivatives. The stability theory also predicts that a small fourth order dissipative term $h^3\Delta^2 u_t$ can control the de-stabilizing effects of high order tangential derivatives. The discrete stabilization term $h^3 A^T A(u^n - u^{n-1})/k$ is proposed for the practical computation. This term can be evaluated all the way up to the boundary so no extra numerical boundary conditions are necessary. After discretization in space, the system of second order ordinary differential equations is integrated in time using a second or fourth order explicit method. Improved spatial accuracy can be achieved away from the boundary by adding a fourth order spatial correction term. Our numerical examples indicate that the resulting scheme is second order accurate measured in max norm and that the time step can be chosen independently of small grid cells near the boundary. Numerical experiments also show that the amount of dissipation needed to stabilize the scheme is very small and, for smooth boundaries, long-time computations do not show any accumulation of the error. A simple modification of the scheme in the vicinity of corners is proposed, but more work is needed to fully understand its implications.

Work is underway to generalize the proposed method to Maxwell's equations written as a system of second order wave equations, which requires more complicated boundary

conditions to be satisfied. Further work is also planned to extend the method to three space dimensions.

A Computing $A^T\boldsymbol{u}$

Using standard notation for an $N \times N$ matrix $\mathcal{A}$ and vectors $\boldsymbol{u}$ and $\boldsymbol{v}$, the most straight forward way of computing $\boldsymbol{v} = \mathcal{A}^T\boldsymbol{u}$ might be

$$v_i = \sum_{j=1}^{N} \mathcal{A}_{j,i} u_j.$$

However, when the matrix is sparse, it is inefficient to store all matrix elements explicitly. If we let $\boldsymbol{a}_i^T$ denote the i'th row of $\mathcal{A}$, we can write $\mathcal{A}$ in row form:

$$\mathcal{A} = \begin{pmatrix} \boldsymbol{a}_1^T \\ \boldsymbol{a}_2^T \\ \vdots \\ \boldsymbol{a}_N^T \end{pmatrix}, \quad \mathcal{A}^T = (\boldsymbol{a}_1, \boldsymbol{a}_2, \ldots, \boldsymbol{a}_N), \tag{81}$$

and $\boldsymbol{v} = \mathcal{A}^T\boldsymbol{u} = \sum_{j=1}^{N} \boldsymbol{a}_j u_j$. Hence, another way of computing $\mathcal{A}^T\boldsymbol{u}$ is by accumulating the contributions from each column of $\mathcal{A}^T$, i.e., each row of $\mathcal{A}$,

1. $\boldsymbol{v} = 0$.
2. for $j = 1, 2, \ldots, N$ do $\boldsymbol{v}$ += $\boldsymbol{a}_j u_j$.

Here the operator += means evaluate right hand side and add the result to the left hand side (as it is defined in the "C" programming language).

Next consider the particular form of the matrix $\mathcal{A} = A$ that arises in our embedded boundary discretization. Away from the boundary, A is defined by (2). Near the boundary, outside points in the stencil get eliminated using the discretized Neumann boundary condition, resulting in a stencil of the type (72). In general, each row of A will only have a few non-zero entries. To simplify the notation, we define $u(k,l) =: u_{k,l}$. Each row of the matrix can then be written in sparse form as

$$A\boldsymbol{u}|_{i,j} =: \sum_{k=1}^{NZ_{i,j}} a_{i,j}^{(k)} u(I_{i,j}^{(k)}, J_{i,j}^{(k)}), \tag{82}$$

where $NZ_{i,j}$ is the number of non-zero entries for the row corresponding to grid point (i,j), and $(I_{i,j}^{(k)}, J_{i,j}^{(k)})$ is the grid point index of the k'th contribution to $A\boldsymbol{u}$ in that row.

Equation (82) represents the matrix A in a sparse row form corresponding to (81). The operation $\boldsymbol{v} = A^T\boldsymbol{u}$ can therefore be computed using the above accumulation algorithm,

1. $\boldsymbol{v} = 0$,

2. for all grid points (i, j) inside Ω do
   for $k = 1, 2, \ldots, NZ_{i,j}$ do

$$v(I_{i,j}^{(k)}, J_{i,j}^{(k)}) \mathrel{+}= a_{i,j}^{(k)} u(i, j).$$

We note that it is only necessary to form the sparse representation of A at interior points where some neighbors are outside Ω. If all neighbors of (i, j) are interior, the "for k"-loop in the second step in the accumulation algorithm can be replaced by

$$\begin{aligned} v(i+1, j) &\mathrel{+}= \frac{u(i,j)}{h^2}, \quad v(i-1, j) \mathrel{+}= \frac{u(i,j)}{h^2}, \quad v(i,j) \mathrel{+}= -\frac{4u(i,j)}{h^2}, \\ v(i, j-1) &\mathrel{+}= \frac{u(i,j)}{h^2}, \quad v(i, j+1) \mathrel{+}= \frac{u(i,j)}{h^2}. \end{aligned}$$

B Proof of Theorem 4

The proof is divided into three cases: $|\lambda| \gg |b|$, $|\lambda| \ll 1$, and $|\lambda| \leq C|b|$.

Case 1, $|\lambda| \gg |b|$: We have $(\lambda - b)/(\lambda + b) \sim 1$. To make the modulus of the right hand side of (71) be close to one,

$$\lambda = Ni\pi + \tilde{\lambda}, \quad |\tilde{\lambda}| << 1, \quad N \geq 1 \text{ integer}.$$

(Note that $N = 0$, i.e., $|\lambda| \ll 1$ is treated in Case 2 below.) To first approximation in $\tilde{\lambda}$,

$$\frac{\tilde{\lambda} + iN\pi - b}{\tilde{\lambda} + iN\pi + b} = 1 + 2\tilde{\lambda}.$$

Therefore,

$$\tilde{\lambda} + iN\pi - b = \tilde{\lambda} + iN\pi + b + 2\tilde{\lambda}^2 + 2iN\pi\tilde{\lambda} + 2b\tilde{\lambda}$$

or

$$\tilde{\lambda}^2 + (iN\pi + b)\tilde{\lambda} + b = 0.$$

Since $|\lambda| \gg |b|$, $|b| \ll N\pi$ and we can expand the roots of $\tilde{\lambda}$ in the small parameter $\epsilon = b/N\pi$, $|\epsilon| \ll 1$,

$$\begin{aligned} \tilde{\lambda} &= -\frac{iN\pi + b}{2} \pm i\frac{N\pi}{2}\sqrt{1 - \frac{4b}{N\pi}\left(\frac{i}{2} - \frac{1}{N\pi} + \frac{b}{4N\pi}\right)} \\ &= -\frac{iN\pi + b}{2} \pm \left(\frac{iN\pi + b}{2} + \frac{ib}{N\pi} + \mathcal{O}(\epsilon^2)\right). \end{aligned}$$

Only the plus sign gives $|\tilde{\lambda}| \ll 1$, and we have

$$\lambda = iN\pi + \tilde{\lambda} \approx iN\pi + \frac{ib}{N\pi}.$$

By solving the characteristic equation (63) for s and inserting the above expression for λ,

$$s = -\frac{a}{2} \pm \sqrt{\frac{a^2}{4} - \omega^2 - N^2\pi^2 - 2b - \frac{b^2}{(N\pi)^2}}. \tag{83}$$

We assume that

$$0 \le \alpha \le 1. \tag{84}$$

Since $|\omega h| \le 1$, we have that

$$|a| \le |\omega|, \tag{85}$$

so $N^2\pi^2 + \omega^2 - a^2/4$ is real and positive. Because $|b|/N\pi \ll 1$, we can expand the roots of (83),

$$\begin{aligned} s &= -\frac{a}{2} \pm i\sqrt{\left(N^2\pi^2 + \omega^2 - \frac{a^2}{4}\right)}\sqrt{1 + \frac{2b}{N^2\pi^2 + \omega^2 - a^2/4}\left(1 + \frac{b}{2N^2\pi^2}\right)} \\ &= -\frac{a}{2} \pm \left(i\sqrt{\left(N^2\pi^2 + \omega^2 - \frac{a^2}{4}\right)} + \frac{ib}{\sqrt{N^2\pi^2 + \omega^2 - a^2/4}} + \dots\right). \end{aligned}$$

We have $ib = -\beta_1\omega^5h^4 + i\beta_2\omega^4h^3$, and $N^2\pi^2 + \omega^2 - a^2/4 \ge 3\omega^2/4$, so

$$\text{Re } s \approx -\frac{1}{2}\alpha h^3\omega^4 \mp \frac{\beta_1\omega^5h^4}{\sqrt{N^2\pi^2 + \omega^2 - a^2/4}} \le -\frac{1}{2}\alpha h^3\omega^4 + \frac{2|\beta_1|\omega^4h^4}{\sqrt{3}}. \tag{86}$$

Therefore, Re $s < 0$ for $\alpha \ge 4|\beta_1|h/\sqrt{3}$, and we conclude that there can be no exponentially growing solutions with $|\lambda| \gg |b|$, when α exceeds that value.

Case 2, $|\lambda| \ll 1$: If $|\lambda| \ll 1$, we can replace (71) by

$$\frac{\lambda - b}{\lambda + b} = 1 + 2\lambda,$$

i.e.,

$$\lambda^2 = -b + \mathcal{O}(b^{3/2}). \tag{87}$$

Then (63) gives us

$$s = -\frac{a}{2} \pm \sqrt{\frac{a^2}{4} - \omega^2 + \lambda^2} \approx -\frac{a}{2} \pm \sqrt{\frac{a^2}{4} - \omega^2 - i\beta_1\omega^5h^4 - \beta_2\omega^4h^3}, \tag{88}$$

and by making the same expansion as above we obtain

$$\text{Re } s \approx -\frac{1}{2}\alpha h^3\omega^4 \pm \frac{|\beta_1|\omega^4 h^4}{\sqrt{3}}.$$

Hence, in this case, Re $s < 0$ for $\alpha > 2|\beta_1|h/\sqrt{3}$, and there can be no exponentially growing solutions with $|\lambda| \ll 1$ when α satisfies that inequality. Note that (87) implies that $|b| \ll 1$ when $|\lambda| \ll 1$.

Case 3, $|\lambda| \le C|b|$: From Case 2 above, we know that $|b| \ll 1$ when $|\lambda| \ll 1$. We can therefore assume $|b| \ge \delta_1 > 0$. Since $|b| = \omega^4 h^3 \sqrt{\beta_2^2 + \beta_1^2\omega^2 h^2}$ and $|\omega h| \le 1$,

$$c_1 h^{-3/4} \le |\omega| \le h^{-1}. \tag{89}$$

Let us define a complex number ρ such that

$$\lambda + b = \rho b, \tag{90}$$

that is, $|\rho - 1| \le C$. There are two possibilities:

$$\text{a) } |\rho| \ge \delta > 0, \quad \text{b) } |\rho| \le \epsilon \ll 1.$$

For possibility a), we start by deriving a bound for Re λ. Let $\lambda_r = \text{Re}\,\lambda$ and $\lambda_i = \text{Im}\,\lambda$. From (71)

$$e^{2\lambda_r} = \left|\frac{\lambda + b - 2b}{\lambda + b}\right| \le 1 + \left|\frac{2b}{\lambda + b}\right| = 1 + \frac{2}{|\rho|} \le 1 + \frac{2}{\delta},$$

and therefore

$$\lambda_r \le \frac{1}{2}\log\left(1 + \frac{2}{\delta}\right) = c_2. \tag{91}$$

By solving the characteristic equation (63) for s, we have

$$s = -\frac{a}{2} \pm \sqrt{\frac{a^2}{4} - \omega^2 - \lambda_i^2 + 2i\lambda_i\lambda_r + \lambda_r^2}.$$

Since (89) bounds $|\omega|$ from below, $\lambda_r^2 \ll \omega^2$. Hence, we can neglect this term, expand the roots of s as before, and use (91) to get

$$\text{Re } s \le -\frac{1}{2}\alpha h^3\omega^4 + \frac{c_2|\lambda_i|}{\sqrt{\frac{3}{4}\omega^2 + \lambda_i^2}}.$$

Let $\rho_r = \text{Re}\,\rho$ and $\rho_i = \text{Im}\,\rho$. The relation (90) gives $\lambda_i = \xi\omega^4 h^3$, where the real valued coefficient $\xi = \rho_i\beta_2 + (\rho_r - 1)\beta_1\omega h$. Clearly, for all $|\rho| \ge \delta$ and $|\omega h| \le 1$,

$$\frac{|\lambda_i|}{\sqrt{\frac{3}{4}\omega^2 + \lambda_i^2}} = \frac{|\xi||\omega h|^3}{\sqrt{\frac{3}{4} + \xi^2\omega^6 h^6}} \le c_3|\omega h|^3.$$

Since $|\omega|$ is bounded from below by (89), $\mathrm{Re}\, s < 0$ for $\alpha > 2c_2c_3c_1^{-1}h^{3/4}$.

For possibility b), we exploit that $\mathrm{Re}\,\lambda > 0$ for $\mathrm{Re}\, s > 0$. We have

$$\lambda = -b(1-\rho), \quad |\rho| \ll 1. \tag{92}$$

When $\rho = 0$, this case reverts to (64) and the half-plane problem. For $\beta_2 > 0$, $\mathrm{Re}\,(-b) = -\beta_2\omega^4h^3 < 0$, but $\mathrm{Re}\,\lambda > 0$ for $\mathrm{Re}\, s > 0$, which is contradicted by (92). Hence there are no solutions with $\mathrm{Re}\, s > 0$ when $\beta_2 > 0$. When $\beta_2 < 0$, $\beta_1 \ll 1$, $|\beta_2| \ll 1$, Theorem 3 applies and the problem can be stabilized by a small amount of dissipation $\alpha \geq K|\beta_1\beta_2|$.

For the perturbed case, $|\rho| = \epsilon$, $\epsilon \ll 1$, a simple computation yields

$$\mathrm{Re}\,(-b+\rho b) = (-1+\rho_r)\beta_2\omega^4h^3 - \rho_i\beta_1\omega^5h^4,$$

and $\mathrm{Re}\,(-b+\rho b) < 0$ if $(-1+\rho_r)\beta_2 + |\rho_i\beta_1| < 0$, i.e.,

$$\beta_2 > \frac{|\rho_i|}{1-\rho_r}|\beta_1| \approx \epsilon|\beta_1|. \tag{93}$$

Hence, when $|\rho| \leq \epsilon$, there can not be any solutions with $\mathrm{Re}\, s > 0$ when (93) is satisfied. For $\beta_2 < \epsilon|\beta_1|$, we can apply the same expansion as in Theorem 3 for the half-plane problem. Since λ is perturbed by $\rho b = \mathcal{O}(\epsilon)$, the roots of s can only be perturbed by $\mathcal{O}(\epsilon)$ and the amount of dissipation necessary to stabilize the problem remains essentially the same.

This concludes the proof of Theorem 4.

References

[1] Gary C. Cohen. *Higher-Order Numerical Methods for Transient Wave Equations*. Springer, 2002.

[2] H.-O. Kreiss, N. A. Petersson, and J. Yström. Difference approximations for the second order wave equation. *SIAM J. Numer. Anal.*, 40:1940–1967, 2002.

[3] R. Weller and G. H. Shortley. Calculation of stresses within the boundary of photoelastic models. *J. Appl. Mech.*, 6:A–71–A–78, 1939.

[4] L. Collatz. *The numerical treatment of differential equations*. Springer verlag, third edition, 1960.

[5] R. B. Pember, J. B. Bell, P. Collella, W. Y. Crutchfield, and M. Welcome. An adaptive Cartesian grid method for unsteady compressible flow in irregular regions. *J. Comput. Phys.*, 120:278, 1995.

[6] C. Zhang and R. LeVeque. The immersed interface method for acoustic wave equations with discontinuous coefficients. *Wave motion*, 25:237–263, 1997.

[7] A. Ditkowski, K. Dridi, and J. S. Hesthaven. Convergent Cartesian grid methods for Maxwell's equations in complex geometries. *J. Comput. Phys.*, 170:39–80, 2001.

[8] Hans Johansen and Philip Colella. A Cartesian grid embedded boundary method for Poisson's equation on irregular domains. *J. Comput. Phys.*, 147:60–85, 1998.

[9] P. Colella. Volume-of-fluid methods for partial differential equations. In E. F. Toro, editor, *Godunov Methods: Theory and Applications*, pages 161–177. Kluwer academic/plenum publishers, New York, 2001.

[10] H.-O. Kreiss and L. Wu. On the stability definition of difference approximations for the initial boundary value problem. *Appl. Num. Math.*, 12:213–227, 1993.

[11] H.-O. Kreiss. Difference approximations for boundary and eigenvalue problems for ordinary differential equations. *Math. Comput.*, 26, 1972.

[12] B. Gustafsson, H.-O. Kreiss, and J. Oliger. *Time dependent problems and difference methods*. Wiley–Interscience, 1995.

[13] R. F. Warming and B. J. Hyett. The modified equation approach to the stability and accuracy analysis of finite-difference methods. *J. Comput. Phys.*, 14:159–179, 1974.

[14] R. J. LeVeque. *Numerical methods for conservation laws*. Birkhäuser, 1992. pp. 117-118.

[15] H.-O. Kreiss and J. Lorenz. *Initial-Boundary Value Problems and the Navier-Stokes Equations*. Academic Press, 1989.

[16] M. Sussman, P. Smereka, and S. Osher. A level set approach for computing solutions to incompressible two-phase flow. *J. Comput. Phys.*, 114(1):146–159, 1994.

University of California
Lawrence Livermore National Laboratory
Technical Information Department
Livermore, CA 94551